Synaptic enrichment and dynamic regulation of the two opposing dopamine receptors within the same neurons

Shun Hiramatsu[1], Kokoro Saito[1], Shu Kondo[2], Hidetaka Katow[3], Nobuhiro Yamagata[4], Chun-Fang Wu[5], Hiromu Tanimoto[1]

[1] Graduate School of Life Sciences, Tohoku University.
[2] Department of Biological Science and Technology, Faculty of Advanced Engineering, Tokyo University of Science.
[3] Department of Cell Biology, New York University.
[4] Faculty and Graduate School of Engineering Science, Akita University.
[5] Department of Biology, University of Iowa.

Abstract

Dopamine can play opposing physiological roles depending on the receptor subtype. In the fruit fly *Drosophila melanogaster*, *Dop1R1* and *Dop2R* encode the D_1- and D_2-like receptors, respectively, and are reported to oppositely regulate intracellular cAMP levels. Here, we profiled the expression and subcellular localization of endogenous Dop1R1 and Dop2R in specific cell types in the mushroom body circuit. For cell-type-specific visualization of endogenous proteins, we employed reconstitution of split-GFP tagged to the receptor proteins. We detected dopamine receptors at both presynaptic and postsynaptic sites in multiple cell types. Quantitative analysis revealed enrichment of both receptors at the presynaptic sites, with Dop2R showing a greater degree of localization than Dop1R1. The presynaptic localization of Dop1R1 and Dop2R in dopamine neurons suggests dual feedback regulation as autoreceptors. Furthermore, we discovered a starvation-dependent, bidirectional modulation of the presynaptic receptor expression in the PAM and PPL1 clusters, two distinct subsets of dopamine neurons, suggesting regulation of appetitive behaviors. Our results highlight the significance of the co-expression of the two opposing dopamine receptors in the spatial and conditional regulation of dopamine responses in neurons.

Introduction

Neurotransmitters typically have multiple cognate receptors, and they may recruit different second messenger systems. Therefore, the expression and localization of receptor subtypes are critical for determining cellular responses to neurotransmitter inputs. The dopaminergic system offers an ideal *in-vivo* study case to this end, as it regulates a wide array of physiological functions through combinations of different receptor subtypes. In mammals, D_1-like receptors are coupled with $G\alpha_s$, thereby activating adenylate cyclase upon ligand binding, whereas $G\alpha_i$-coupled D_2-like receptors inhibit cyclase activity (Beaulieu & Gainetdinov, 2011). Four dopamine receptors have been identified in *Drosophila*: *Dop1R1*, *Dop1R2*, *Dop2R*, and *DopEcR* (K. A. Han et al., 1996; Hearn et al., 2002; Srivastava et al., 2005; Sugamori et al., 1995). *Dop1R1* and *Dop2R*, also known as *DopR1*, *dDA1* and *dumb*, and as *DD2R*, respectively, correspond to the D_1- and D_2-like receptors, respectively (Hearn et al., 2002; Sugamori et al., 1995). Dop1R2 and DopEcR are invertebrate-specific and have been reported to recruit different second messenger systems (K. A. Han et al., 1996; Srivastava et al., 2005). Intriguingly, recent data of single-cell RNA-seq and transgenic expression profiling revealed that the expression of these dopamine receptors is highly overlapping in the fly brain (Croset et al., 2018; Davie et al., 2018; Kondo et al., 2020), unlike the spatially segregated expression of the D_1- and D_2-like receptors in vertebrate brains (Gerfen & Surmeier, 2011). Considering the opposing physiological roles of the Dop1R1 and Dop2R, their protein localization, especially in those cells where they are co-expressed, should be critical to determine the responses to the dopamine inputs.

Drosophila mushroom bodies (MB) have long served as a unique dopaminergic circuit model to study adaptive behaviors, such as associative learning. MB-projecting neurons and their connections have been systematically described at both mesoscopic and ultrastructural resolutions (Aso, Hattori, et al., 2014; Li et al., 2020; Takemura et al., 2017; Tanaka et al., 2008). Kenyon cells (KCs), the major MB intrinsic neurons, encode a variety of sensory information (Honegger et al., 2011; Turner et al., 2008; Vogt et al., 2014). Intriguingly, each KC receives synaptic inputs from different dopaminergic projections in multiple spatially segmented compartments along its axon in the MB lobe (Aso, Hattori, et al., 2014; Tanaka et al., 2008). MB-projecting dopamine neurons (DANs) originate from the three cell clusters (Mao & Davis, 2009; Nässel & Elekes, 1992). DANs in the protocerebral posterior lateral 1 (PPL1) cluster project to the vertical lobes and the peduncle of the MB, and they control different aspects of associative memory (Aso et al., 2010, 2012; Aso & Rubin, 2016; Claridge-Chang et al., 2009; Krashes et al., 2009; Mao & Davis, 2009; Masek et al., 2015; Riemensperger et al., 2005; Takemura et al., 2017; Vogt et al., 2014). The protocerebral anterior medial (PAM) cluster, the largest DAN cluster, mostly projects to the

62 medial lobes of the MB, and many PAM neurons are involved in reward processing (Burke et al.,
63 2012; Felsenberg et al., 2018; Huetteroth et al., 2015; Ichinose et al., 2021; Lin et al., 2014; Liu
64 et al., 2012; Yamagata et al., 2015, 2016). DANs in PPL2ab project to the MB calyx and control
65 the conditioned odor response (Boto et al., 2019). In addition to the variety of the dopamine
66 sources, KCs express all four dopamine receptor subtypes (Deng et al., 2019; Kondo et al., 2020).
67 Besides KCs, these lobe-projecting DANs have synaptic outputs to multiple types of neurons,
68 including MBONs, APL and DPM (Li et al., 2020; Takemura et al., 2017; Zhou et al., 2019).
69 Given the multitude of modulatory effects of dopamine in the MB (Berry et al., 2018; Cohn et al.,
70 2015; Handler et al., 2019), receptor localization in each cell type provides important information
71 for interpreting such functional diversity.

72 The projections and synapses of the neurons in the MB circuit are tightly intertwined (Li
73 et al., 2020; Takemura et al., 2017). Therefore, conventional immunohistochemical approaches
74 using light microscopy do not allow identification of cells from which immunoreactive signals
75 originate. Precise determination of their subcellular localization requires conditional visualization
76 of the proteins of interest only in the target MB neurons (Bonanno et al., 2024; Fendl et al., 2020;
77 Sanfilippo et al., 2024). Employing the CRISPR/Cas9-mediated split-GFP tagging strategy (D.
78 Kamiyama et al., 2016; R. Kamiyama et al., 2021; Kondo et al., 2020), we profiled the spatial
79 distribution of endogenous Dop1R1 and Dop2R proteins in KCs, the PAM, and the PPL1 DANs.

Results

Co-expression of *Dop1R1* and *Dop2R* genes in the adult *Drosophila* brain

To compare the expression of different dopamine receptor genes in detail, we used T2A-GAL4 knock-ins of the endogenous *Dop1R1* and *Dop2R* genes (Kondo et al., 2020) with fluorescent reporters. Both lines labelled many neuropils including the MB (Figure 1A and 1B), and the overlapping expression of these receptors is consistent with our previous quantification of GAL4-positive cells for both genes (58,049 and 68,528 for *Dop1R1* and *Dop2R*, respectively, out of 118,331 brain cells; Kondo et al., 2020). Double labelling of *Dop1R1-T2A-LexA* and *Dop2R-T2A-GAL4* expression revealed cells with overlapping and differential patterns (Figure 1C-1I; see also Kondo et al., 2020). We confirmed the co-expression of *Dop1R1* and *Dop2R* in the KCs (Figure 1 – figure supplement 1) as reported previously (Kondo et al., 2020). The PAM cluster of DANs expressed both *Dop1R1* and *Dop2R* (Figure 1C and 1D). On the other hand, most of the DANs in the PPL1 cluster strongly expressed *Dop2R*, but *Dop1R1* only weakly (Figure 1C and 1E). We further found that *Dop1R1*, but not *Dop2R*, was highly expressed in the ring neurons projecting to the ellipsoid body (Figure 1G and 1H; Hanesch et al., 1989) and the neuropil ensheathing glia (Figure 1I; Awasaki et al., 2008). In conclusion, *Dop1R1* and *Dop2R* genes are co-expressed in PAM neurons and KCs but have selective expressions in other cell types.

Quantification of subcellular enrichment of endogenous proteins in target cells

The overlapping expression of *Dop1R1* and *Dop2R* genes prompted us to examine the subcellular localization of these receptor proteins. To elucidate the localization of these broadly expressed receptors (Figure 1), we took advantage of split-GFP tagging of endogenous proteins (D. Kamiyama et al., 2016; Kondo et al., 2020). By adding seven copies of GFP_{11} tags to the C-termini of the Dop1R1 and Dop2R proteins, their intracellular distribution can be visualized specifically in cells expressing GFP_{1-10} through split-GFP reconstitution (Figure 2A). To verify the functional integrity of reconstituted GFP (rGFP)-fused receptors, we examined aversive olfactory memory of homozygous flies carrying GFP_{11}-tagged dopamine receptors and induced GFP reconstitution in KCs. Both Dop1R1 and Dop2R have been shown to be required for aversive memory in α/β and γ KCs (Kim et al., 2007; Scholz-Kornehl & Schwärzel, 2016). Memory scores of the rGFP-fused receptor flies were comparable to that of control flies without GFP_{11} insertion (Figure 2 – figure supplement 1).

To quantify the subcellular enrichment of the receptors, we devised Localization Index (LI). Briefly, LI is the normalized ratio of the rGFP signal to the reference membrane marker

112 signal (CD4::tdTomato). If the target and reference proteins had the identical distribution, LI
113 would be 1 everywhere. More or less enrichment of rGFP would result in the LI larger or smaller
114 than 1, respectively (Figure 2C; see also Methods for detail). For visualization, the reference
115 membrane signal was color-coded with LI (Figure 2C). As proof of principle, mapping the LI of
116 DopEcR::rGFP signals in KCs highlighted enrichment in the proximal peduncle (Figure 2B and
117 2C), which is consistent with the previous report (Kondo et al., 2020). This representation thus
118 visualizes the subcellular enrichment of the targeted receptors in the plasma membrane of GAL4-
119 expressing cells.

120 **Colocalization of Dop1R1 and Dop2R proteins**

121 First, we compared the localization of Dop1R1 and Dop2R proteins in KCs, where both receptor
122 genes were highly expressed (Figure 1 – figure supplement 1). These receptors were distributed
123 throughout KC membranes with predominant enrichment in the lobes (Figure 3A-3C), but
124 sparsely in the calyx (Figure 3B and 3C). LI quantification revealed that enrichment in the lobes
125 was more pronounced in Dop2R compared to Dop1R1, whereas localization to the calyx was
126 sparser in Dop2R than Dop1R1 (Figure 3D). We confirmed that the differential localization of
127 these receptors was consistent across multiple experimental batches conducted on different days
128 (Figure 3 - figure supplement 1).

129 KCs have major presynaptic sites in the MB lobes, where Dop1R1 and Dop2R are
130 enriched (Figure 3A-3D). Therefore, we examined receptor localization with the reference of Brp
131 immunostaining, which labels the active zones (AZ) (Wagh et al., 2006). To distinguish the AZ
132 in KCs from those in the other neurons, we co-labeled the plasma membrane of KCs and
133 conducted high-magnification imaging using Airyscan. At this resolution, Brp puncta in KCs and
134 those from non-KCs could be distinguished based on their overlap with the KC membrane marker
135 (Figure 4B and 4C). Interestingly, KC-specific visualization of Dop1R1 and Dop2R proteins
136 revealed signals around the Brp puncta of the same cells, suggesting presynaptic localization
137 (Figure 4B and 4C). Additionally, we found the receptor condensates adjacent to the Brp clusters
138 of non-KCs, suggesting their localization at the postsynaptic sites (Figure 4B and 4C). The
139 synaptic receptor localization is consistent in different subsets of KCs (α/β and γ; Figure 4A-4C).
140 In conclusion, both of these antagonizing dopamine receptors are enriched in the presynaptic and
141 postsynaptic sites of KCs (Figure 4D).

142 To further clarify the presynaptic localization in KCs, we labeled the AZ of KCs by
143 expressing *Brp^{short}::mStraw* (Fouquet et al., 2009) and confirmed that both Dop1R1::rGFP and
144 Dop2R::rGFP were associated with the Brp puncta in the lobes (Figure 5A, Figure 5 – figure

145 supplement 1). Interestingly, we found that not all Brp puncta of KCs were associated with the
146 dopamine receptors (Figure 5A), suggesting that dopaminergic presynaptic modulation is
147 heterogeneous across release sites. This heterogeneity can well explain differential learning-
148 induced plasticity across boutons within single KCs (Bilz et al., 2020; Davidson et al., 2023).
149 To better resolve the presynaptic localization of Dop1R1 and Dop2R, we turned to "giant"
150 *Drosophila* neurons differentiated from cytokinesis-arrested neuroblasts in culture (Wu et al.,
151 1990). The expanded size of the giant neurons is advantageous for investigating the microanatomy
152 of neurons in isolation (Saito & Wu, 1991; Wu et al., 1990; Yao et al., 2000). Importantly, these
153 giant neurons exhibit characteristics of mature neurons, including firing patterns (Wu et al., 1990;
154 Yao & Wu, 2001; Zhao & Wu, 1997) and acetylcholine release (Yao et al., 2000), both of which
155 are regulated by cAMP and CaMKII signaling (Yao et al., 2000; Yao & Wu, 2001; Zhao & Wu,
156 1997). In the giant neurons from the *Brp::SNAP* embryos (Kohl et al., 2014), Brp was localized
157 to the terminals of neurites, but rarely in the proximal neurites (Figure 5B). Furthermore, we found
158 punctate Brp clusters in the giant neuron terminals (Figure 5B), together recapitulating the
159 essential characteristics of the AZ cytomatrix in adult neurons. To confirm if dopamine receptors
160 localize to these presynaptic sites, we generated the giant neurons from embryos carrying the
161 Venus insertion to *Dop1R1* and *Dop2R* (Kondo et al., 2020) together with *Brp::SNAP*. Both
162 Dop1R1 and Dop2R were expressed in the giant neurons and enriched in the same distal axonal
163 segments (Figure 5C). A closer investigation revealed that these receptors are associated with the
164 Brp clusters (Figure 5C). These observations in the giant neurons are strikingly similar to those
165 in the KCs (Figure 3, 4 and 5A), corroborating that the presynaptic localization of these receptors
166 is independent of the circuit context.

167 **Distinct subcellular enrichment of dopamine receptors in MBONs and DANs**

168 Presynaptic and postsynaptic localization of Dop1R1 and Dop2R in KCs prompted us to
169 investigate MBONs, that have profound postsynaptic contacts with DANs in the MB
170 compartments (Li et al., 2020; Takemura et al., 2017). MBON-γ1pedc>αβ (also known as MB-
171 MVP2, MBON-11; Aso, Hattori, et al., 2014; Tanaka et al., 2008) has most of its postsynaptic
172 sites on the γ1 compartment and the peduncle of the α/β neurons and send axonal projections to
173 the α and β lobes (Figure 6; Dorkenwald et al., 2024; Schlegel et al., 2024). We analyzed the
174 subcellular localization of Dop1R1::rGFP and Dop2R::rGFP in MBON-γ1pedc>αβ by driving
175 GFP_{1-10} using *R83A12-GAL4* (Perisse et al., 2016). Strikingly, both Dop1R1 and Dop2R are
176 enriched in the dendritic projection in the γ1 compartment (Figure 6B and 6C) in sharp contrast
177 to the sparse distribution of these receptors in the dendrites of KCs (Figure 3B-3D). This

178 localization is consistent with previous reports of functional DAN>MBON synapses (Takemura
179 et al., 2017) and dopaminergic plasticity on the dendrites (Boto et al., 2019; Pribbenow et al.,
180 2022). Additionally, we detected these receptors in the presynaptic boutons (Figure 6C), which
181 are consistent with the results in KCs and in the giant neurons (Figure 4B, 4C, 5A and 5C).

182 D_2-like receptors in mammals are expressed in DANs and act as autoreceptors, which
183 mediates feedback signals by receiving neurotransmitters released from the neuron on which the
184 receptors reside (Ford, 2014). In *Drosophila*, multiple dopamine receptor genes are expressed in
185 DANs (Figure 1D and 1E; Aso et al., 2019; Deng et al., 2019; Kondo et al., 2020), but it is unclear
186 if these receptors function as autoreceptors. We therefore examined the subcellular localization
187 of Dop1R1 and Dop2R in the PAM cluster DANs with a particular focus on their presynaptic
188 terminals. The PAM neurons are polarized; presynaptic proteins are abundantly enriched in the
189 MB lobe and barely detected in dendrites (Figure 7A and 7B). We visualized Dop1R1 and Dop2R
190 proteins in the PAM cluster DANs using *R58E02-GAL4*, and both were localized to the terminals
191 in the MB lobes (Figure 7C). Representation of LI for Dop1R1 and Dop2R in the PAM neurons
192 again showed stronger presynaptic enrichment of Dop2R than Dop1R1 (Figure 7C). Dop2R was
193 strongly enriched at β'1 compartment showing significantly higher LI than Dop1R1 (Figure 7D
194 and 7E). Higher magnification revealed the accumulation of both Dop1R1 and Dop2R in the
195 boutons (Figure 7F). The presynaptic localization of Dop1R1 and Dop2R in DANs suggests that
196 both receptors mediate feedback regulation.

197 **State-dependent and bidirectional modulation of dopamine receptor expression in the PAM**
198 **and PPL1 DANs**

199 The activity of MB-projecting DANs is reported to be dynamic and sensitive to feeding states
200 (Ichinose et al., 2017; Liu et al., 2012; Plaçais & Preat, 2013; Senapati et al., 2019; Siju et al.,
201 2020; Tsao et al., 2018; Yamagata et al., 2016). We therefore examined if starvation alters the
202 protein expression of Dop1R1 and Dop2R in these MB-projecting DANs (Figure 8A). We found
203 a significant elevation of Dop1R1 in the terminals of PAM-γ5 upon starvation for 10 hours or
204 longer (Figure 8B and 8C). In contrast, starvation did not increase Dop2R in PAM-γ5 but rather
205 tended to decrease, if at all (Figure 8B and 8C). We found similar starvation-dependent changes
206 in Dop1R1 and Dop2R levels in other PAM neurons (Figure 8 – figure supplement 1A-1D). These
207 results together suggest that starvation enhances presynaptic dopamine signaling in the reward-
208 related PAM neurons by shifting the balance of Dop1R1 and Dop2R.

209 DANs of the PAM and PPL1 clusters exert distinct, largely opposite behavioral functions
210 (Claridge-Chang et al., 2009; Liu et al., 2012). Therefore, plasticity in the PPL1 neurons may

211 differ from that in the PAM neurons. To test this hypothesis, we examined the starvation-
212 dependent change in Dop1R1 and Dop2R protein expression in the PPL1 neurons. To this end,
213 we visualized GFP_{11}-tagged receptors by expressing GFP_{1-10} using *TH-GAL4* (Friggi-Grelin et al.,
214 2003). We detected Dop2R proteins in all MB projections of the PPL1 neurons, whereas Dop1R1
215 proteins were only detectable in the terminals of the PPL1-α3 neuron (Figure 8D). Strikingly, the
216 starvation-induced changes in the PPL1 neurons were opposite to those in the PAM: Dop2R, but
217 not Dop1R1, was significantly increased in the α3 compartment (Figure 8E and 8F). In the other
218 compartments, the Dop2R::rGFP levels tended to be higher in starved flies although the increase
219 was not statistically significant (Figure 8 – figure supplement 1E and 1F). These results are in line
220 with the state-dependent changes in the physiology of these DANs (Siju et al., 2020; Tsao et al.,
221 2018). Taken together, starvation induces bidirectional modulation of the dual autoreceptor
222 system in the PPL1 and PAM DANs, and we propose that these changes shift the balance of
223 dopamine output from these subsets (Figure 9A).
224 The dopaminergic signals from the PPL1 neurons inhibit expression of appetitive
225 olfactory memory in fed flies (Krashes et al., 2009; Pavlowsky et al., 2018). The increased Dop2R
226 autoreceptors in starved flies (Figure 8E and 8F) may thus disinhibit appetitive memory
227 expression by suppressing PPL1 outputs (Figure 9B). To test this hypothesis, we examined
228 appetitive memory by transgenic knockdown of Dop2R specifically in the PPL1 cluster neurons
229 using *MB504B-GAL4* (Vogt et al., 2014). Indeed, appetitive memory was impaired (Figure 9C),
230 suggesting the significance of the negative feedback regulation of the PPL1 via Dop2R in
231 appetitive behavior expression. This result is consistent with our model, which suggests that
232 enhanced negative feedback to PPL1 via Dop2R in the starved state contributes to the expression
233 of appetitive behavior (Figure 9A and 9B).

Discussion

The present study demonstrated the expression, subcellular localization, and dynamics of endogenous dopamine receptors, specifically Dop1R1 and Dop2R, in the MB circuit of the fly brain. Compared to intronic insertions of reporters using transposons (Fendl et al., 2020), CRISPR/Cas9-based insertion is advantageous in terms of flexibility in fusion sites (Bonanno et al., 2024; R. Kamiyama et al., 2021; Sanfilippo et al., 2024; Williams et al., 2019). This enables the C-terminal tagging of dopamine receptors that do not perturb protein localization and function (Figure 2 – figure supplement 1).

The split-GFP reconstitution strategy enables sensitive detection of low-abundant endogenous proteins by the tandem multimerization of the GFP_{11} tags, as shown in other epitope tags such as SunTag and smFPs (Tanenbaum et al., 2014; Viswanathan et al., 2015). The native fluorescence of rGFP was sufficient to detect tagged proteins at the high signal-to-noise ratio, without the need for signal amplification using antibodies. The background fluorescence of the split-GFP fragments was practically negligible (Figure 8D; D. Kamiyama et al., 2016; Kondo et al., 2020). This approach can thus be applicable to monitor localization and dynamics of endogenous proteins of low abundance.

Our cell-type-specific receptor labeling offers further potential for ultrastructural examination using higher resolution imaging techniques. For example, synaptic condensates of Dop1R1 and Dop2R at the resolution in this study (Figures 4 and 5) did not allow us to distinguish the receptors on the plasma membrane and those that are internalized (Dumartin et al., 1998; Kotowski et al., 2011). Thus, application of super-resolution fluorescent imaging and expansion microscopy (Gao et al., 2019) would disentangle the precise membrane localization of the receptors.

Spatial regulation of dopamine signaling through the two opposing receptors

How do Dop1R1 and Dop2R function in presynaptic terminals? Released dopamine is not confined to the synaptic cleft, but diffused in the extracellular space (Liu et al., 2021; Rice & Cragg, 2008). Such volume transmission can increase the number of target synapses by 10 times (Li et al., 2020; Takemura et al., 2017). Thus, the broader distribution of Dop1R1 (Figure 3B-3D and 7C-7E) may enable it to respond to extrasynaptic dopamine. In response to residual dopamine, Dop2R at the AZ may inhibit activities of adenylate cyclases and voltage-gated calcium channels (Beaulieu & Gainetdinov, 2011; Hearn et al., 2002), thereby reducing the noise of the second messengers. Collectively, the spatial configuration of Dop1R1 and Dop2R may enhance the sensitivity and precision of dopaminergic modulation.

Furthermore, presynaptic receptor localization (Figure 4B-4D, 5A, 5C, 6C and 7F)

267 suggests a spatially confined cAMP, forming nanodomains (Anton et al., 2022; Bock et al., 2020;
268 Maiellaro et al., 2016; Zhang et al., 2020). cAMP signaling has been shown to regulate multiple
269 events at presynaptic terminals, such as the molecular assembly at the AZ and synaptic vesicle
270 dynamics (Ehmann et al., 2018; Kittel & Heckmann, 2016; Kuromi & Kidokoro, 2000, 2005;
271 Maiellaro et al., 2016; Renger et al., 2000; Sachidanandan et al., 2023). Especially in KCs, cAMP-
272 dependent plasticity underlies associative memory (Boto et al., 2014; Cohn et al., 2015; Louis et
273 al., 2018; Noyes & Davis, 2023; Stahl et al., 2022). Presynaptic cAMP regulation through
274 Dop1R1 and Dop2R therefore explains the requirement of these receptors in associative memory
275 (Kim et al., 2007; Scholz-Kornehl & Schwärzel, 2016).

276 **The dual autoreceptor system may shape dopamine release**

277 Presynaptic localization of Dop1R1 and Dop2R in DANs (Figure 7C-7F) strongly
278 suggests their functions as autoreceptors. In the *Drosophila* nervous system, Dop2R was shown
279 to negatively regulate dopamine release (Shin & Venton, 2022; Vickrey & Venton, 2011). Tight
280 presynaptic enrichment in PAM (Figure 7F) suggests that Dop2R receives high levels of
281 dopamine and effectively prevents overactivation. The presence of Dop1R1 in DAN terminals
282 (Figure 7F) was unexpected and introduces another layer of presynaptic regulations to dopamine
283 release. Although it must be functionally verified, presynaptic Dop1R1 likely provides positive
284 feedback to the dopamine release as an autoreceptor. This positive feedback would be particularly
285 important for signal amplification when extracellular dopamine concentrations are low.
286 Consistent this hypothesis, presynaptic Dop1R1 was undetectable in most PPL1 DANs (Figure
287 8D), which were reported to have high spontaneous activities (Feng et al., 2021; Plaçais & Preat,
288 2013). Taken together, this dual autoreceptor system likely fine-tune the amplitude and kinetics
289 of dopamine release. Alternatively, these presynaptic receptors could potentially receive
290 extrasynaptic dopamine released from other DANs. Therefore, the autoreceptor functions need to
291 be experimentally clarified by manipulating the receptor expression in DANs.

292 Dopamine receptor expression is reported to be associated with prolonged exposure to
293 psychoactive substances, such as caffeine and ethanol (Andretic et al., 2008; Kanno et al., 2021;
294 Kondo et al., 2020; Petruccelli et al., 2018). Our study further showed starvation-dependent
295 changes of Dop1R1 and Dop2R in DAN terminals (Figure 8). Strikingly, starvation responses of
296 presynaptic Dop1R1 and Dop2R were differential depending on the DAN cell types (Figure 8).
297 These results indicate that starvation bidirectionally changes the dual autoreceptor system, putting
298 more weight on the PAM output over PPL1 to control the expression of appetitive behavior
299 (Figure 9). This shifted balance explains the state-dependent changes in the presynaptic activity

of these two clusters of DANs (Siju et al., 2020; Tsao et al., 2018) and bidirectional modulation of the MB output (Aso, Sitaraman, et al., 2014; Ichinose et al., 2021; Owald et al., 2015).

302 **Materials and Methods**

303 **Key resource table**

	Source	Identifier
Antibodies and reagents		
Mouse anti-TH	ImmunoStar Inc., Hudson, WI, USA	#22941
Mouse anti-Brp	Developmental Studies Hybridoma Bank, Iowa city, IA, USA	nc82
Rabbit anti-DsRed	Takara Bio USA, Inc., San Jose, CA, USA	#632496
Goat anti-mouse Alexa Fluor 405	Invitrogen, Waltham, MA, USA	#A31553
Goat anti-mouse Alexa Fluor 633	Invitrogen, Waltham, MA, USA	#A21052
Goat anti-rabbit Alexa Fluor 568	Invitrogen, Waltham, MA, USA	#A11036
SNAP-Cell 647-SiR	Ipswich, MA, USA	S9102S
CLIP-Surface 547 substrate	New England Biolabs Inc., Ipswich, MA, USA	#S9233S
RU486 (Mifepristone)	Tokyo Chemical Industory Co., Tokyo, Japan	#M1732
***Drosophila* strain**		
Dop1R1-T2A-GAL4	Kondo et al., 2020	N/A
Dop2R-T2A-GAL4	Kondo et al., 2020	N/A
Dop1R1-T2A-LexA	Kondo et al., 2020	N/A
Dop1R1::7xGFP$_{11}$	Kondo et al., 2020	N/A
Dop2R::7xGFP$_{11}$	Kondo et al., 2020	N/A
DopEcR::7xGFP$_{11}$	Kondo et al., 2020	N/A
Dop1R1::Venus	Kondo et al., 2020	N/A
Dop2R::Venus	Kondo et al., 2020	N/A
UAS-GFP$_{1-10}$	Kondo et al., 2020	N/A
UAS-mCD8::GFP	Pfeiffer et al., 2010	BDSC #32194
lexAop-rCD2::GFP	Miyamoto et al., 2012	N/A
UAS-CD4::tdTomato	C. Han et al., 2011	BDSC #35841
UAS-nSyb::CLIP	Kohl et al., 2014	BDSC #58398
UAS-Brp^{short}::mStraw	Fouquet et al., 2009	N/A
Brp::SNAP	Kohl et al., 2014	BDSC #58397
MB-Switch	Mao et al., 2004	BDSC #81013
OK371-GAL4	Mahr & Aberle, 2006	BDSC #26160
R83A12-GAL4	Jenett et al., 2012	BDSC #40348

R15A04-GAL4	Janett et al., 2012	BDSC #48671
R58E02-GAL4	Jenett et al., 2012	BDSC #41347
TH-GAL4	Friggi-Grelin et al., 2003	N/A
MB504B	Aso, Hattori et al., 2014	BDSC #68329
UAS-Dop2R-RNAi	Perkins et al., 2015	BDSC #50621
Software		
Fiji	Schindelin et al., 2012, http://fiji.sc	RRID: SCR_002285
GraphPad Prism 5	GraphPad Software	RRID: SCR_002798

304

305 **Flies**

306 Flies were raised on standard cornmeal food at 25°C under a 12:12 h light-dark cycle (ZT0 at 8
307 AM) for all experiments. The GAL4-UAS system was used to express the transgenes of interest
308 in specific neuron subtypes. Flies carrying GAL4 were crossed to another strain carrying UAS
309 reporters, and F1 progenies were used in the experiments. To visualize GFP_{11}-tagged dopamine
310 receptors in the specific cell-types, female fly strains carrying *UAS-CD4::tdTomato*, *UAS-GFP*$_{1-}$
311 $_{10}$ and GAL4 driver were crossed to male fly strains carrying *Dop1R1::GFP*$_{11}$ or *Dop2R::GFP*$_{11}$,
312 and F1 progenies were used. To make the giant neuron culture, embryos from *Brp::SNAP* or the
313 F1 progeny of *OK371-GAL4* crossed with *Brp::SNAP, UAS-mCD8::GFP, UAS-nSyb::CLIP* flies
314 were used. For the fly lines used in our manuscript, see Key resource table.

315 **RU486 feeding**

316 To activate Gene-Switch, flies are fed with food containing RU486 (mifepristone). Food
317 containing 200 µM of RU486 was prepared as described previously (Mao et al., 2004). In brief,
318 200 mg of RU486 was dissolved in 10 ml of 99.5% ethanol to make a stock solution. 4.3 µl of the
319 stock solution was added to 1 ml of molten fly food and mixed thoroughly. The molten food with
320 RU486 was poured into vials or bottles and cooled to make solid food.

321 **Brain dissection and Immunohistochemistry**

322 Flies were sorted under CO_2 anesthesia to select males with the specific genotypes and kept in a
323 food vial for recovery at least 24 h prior to the dissection. Fly brains were dissected 3-7 days after
324 eclosion in ice-cold Phosphate-buffered saline (PBS). After dissection, brains were kept in ice-
325 cold PBS with 2% paraformaldehyde (PFA) for up to 30 min. For fixation, brains were incubated

326 in 2 % PFA in PBS for 1 hour at room temperature. Fixed brains were washed in PBS with 0.3 %
327 Triton X-100 (PBT) for 10 min 3 times. For rGFP imaging, fixed brains were mounted in SeeDB2
328 (Ke et al., 2016), and native fluorescence was imaged without signal amplification.
329 For chemical tagging reaction of nSyb::CLIP, brains were incubated in PBT containing
330 CLIP-Surface 547 substrate (1μM) for 15 min at room temperature. Brains were washed in PBT
331 for 10 min 3 times.
332 For immunohistochemistry, fixed brains were blocked in 3 % normal goat serum (NGS;
333 Sigma-Aldrich, G9023) for 30 min at room temperature. Brains were incubated in primary and
334 secondary antibodies diluted in PBT with 1 % NGS over two nights at 4 ℃, respectively. After
335 each step, brains were washed three times in PBT for longer than 20 min at room temperature and
336 mounted in 86% glycerol. The following primary antibodies were used: mouse anti-TH (1:100),
337 mouse anti-Brp (1:40), rabbit anti-DsRed (1:2000). Secondary antibodies: Alexa Fluor 633 goat
338 anti-mouse (1:400 for anti-TH, 1:200 for anti-Brp).

339 **Fluorescent imaging**

340 For image acquisition, whole-mount brains were scanned with the Olympus FV1200 confocal
341 microscope with following objective lens; 20x oil (NA = 0.85, UPLSAPO20XO, Olympus;
342 Figure 1A, 1B, 1G and 1H), 30x silicone (NA = 1.05, UPLSAPO30XS, Olympus; Figure 3B and
343 3C), 40x oil (NA = 1.3, UPLFLN40XO, Olympus; Figure 2B, 2C, 6B, 7A, 7C, 7D, 8B, 8E, Figure
344 8 – figure supplement 1-A,C,E), or 60x oil (NA = 1.42, PLAPON60XO, Olympus; Figure 1D,
345 1E, 1I, Figure 1 – figure supplement 1). Z-stack images were acquired.
346 For high resolution imaging in Figure 4B, 4C, 5A, 6C, 7F and Figure 5 – figure
347 supplement 1, we used Airyscan on Zeiss LSM800 with 63x oil objective lens (NA = 1.40, Plan-
348 Apochromat).

349 **Image analysis**

350 All image analysis were conducted on Fiji (Schindelin et al., 2012).
351 To visualize the subcellular localization of dopamine receptors in defined neurons, we
352 devised the localization index (LI). Relative receptor density was calculated in each voxel by
353 dividing the receptor (reconstituted GFP) signals by the corresponding membrane signals
354 (CD4::tdTomato). To set ROI, any voxels devoid of membrane signal were censored. The local
355 density was normalized by the mean values in the ROI. For the visual representation, the reference
356 membrane signals were colored according to the normalized LI (Figure 2C). To quantify mean LI
357 in each subcellular region (Figure 3H, 7E), ROI was manually set.

358 **Embryonic giant neuron culture**

359 Multinucleated giant neurons from neuroblasts were generated as described previously (Wu et al.,
360 1990). Briefly, the interior of a gastrula from stage 6/7 embryo was extracted with a glass
361 micropipette and dispersed into a drop of culture medium (~ 40 μm) on an uncoated coverslip.
362 The culture medium contained 80% *Drosophila* Schneider's insect medium (S0146-100ML,
363 Merck KGaA, Darmstadt, Germany) and 20% fetal bovine serum (F2442-100ML, Merck KGaA,
364 Darmstadt, Germany), with the addition of 50 μg/ml streptomycin, 50 U/ml penicillin (all from
365 Sigma, St. Louis, MO, USA) and cytochalasin B (CCB; 2 μg/ml; Sigma, St. Louis, MO, USA).
366 CCB was removed by washing with CCB-free medium 1 d after plating. All cultures were grown
367 in a humidified chamber.

368 To label Brp::SNAP, cells were incubated in fluorescent SNAP substrate diluted in the
369 culture medium (1:5000, SNAP-Cell 647-SiR) for half an hour at RT. Subsequently, the same
370 cells were labeled by the SNAP substrate to minimize the crosstalk. After the incubation, cells
371 were washed with the culture medium and subjected to confocal scanning with Leica TCS SP8
372 microscopy equipped with a 40x oil immersion objective (HC PL APO 40x/1.30 Oil PH3 CS2,
373 Leica). Acquired images were then processed with the LIGHTNING software.

374 **Behavioral assays**

375 The experimental protocols for appetitive learning experiment (Figure 9C) were as described
376 previously (Ichinose and Tanimoto., 2016). For appetitive conditioning, a group of approximately
377 50 flies in a training tube alternately received 3-octanol (3OCT; Merck) and 4-
378 methylcyclohexanol (4MCH; Sigma-Aldrich), for 1 minute in a constant air flow with or without
379 reward with an interval of 1 minute between the two odor presentations. These odorants were
380 diluted to 1.2% and 2% with paraffin wax (Sigma-Aldrich), respectively. Dried 2 M sucrose
381 (Sigma-Aldrich) on a piece of filter paper was used as the reward. Flies were starved in the
382 presence of wet tissue paper for 24 hours before appetitive conditioning. For testing, flies were
383 given a choice between the odor paired with reward (Conditioned stimulus, CS+) and another one
384 unpaired (CS-). Their distribution in the plexiglass T-maze was video-recorded one frame per
385 second for 2 minutes with the CMOS cameras (GS3-U3-51S5M, FLIR) under infrared LED
386 illumination (Ichinose & Tanimoto, 2016). Flies were forced to stay on the floor by applying
387 Fluon (Insect-a-Slip PTFE30, BioQuip Products) on the side and top of T-maze arms.

388 Learning index was then calculated by counting the number of flies in each arm using
389 ImageJ macro as described previously (Ichinose and Tanimoto, 2016) with the following formula
390 (Tempel et al., 1983):

$$Learning\ index = \frac{\#_{CS-} - \#_{CS+}}{\#_{CS+} + \#_{CS-}}$$

where $\#_{CS+}$ and $\#_{CS-}$ imply the number of flies in the CS+ and the CS- arms, respectively. Learning index was calculated for every second and was averaged for the last 60 s of the 120 s test session. An average of a pair of reciprocally trained groups was used as a single data point.

In aversive associative learning experiment (Figure 2 – figure supplement 1), flies were conditioned with twelve 1.5 second pulses of 90V electric shock paired with either 4MCH or 3OCT (CS+) for 1 minute. After 1 minute of interval, another odor (CS-) was presented without electric shock for 1 minute. Flies were tested immediately after training. In the test, flies were allowed to choose between the CS+ and CS- odors in a T-maze. The number of flies in each side of the arm (#CS+ and #CS-) after 2 minutes was used to calculate learning index as described above.

Statistics

For multiple comparison (Figure 2 – figure supplement 1, Figure 8C, 8F and Figure 8 – figure supplement 1 and Figure 9C), statistics were performed by Prism5 (GraphPad). Data were always first tested for normality (Shapiro-Wilk test) and for homoscedasticity (Spearman's test or Bartlett's test). If these assumptions were not violated, parametric tests (one- or two-way ANOVA, followed by Dunnett's test or t-test with Bonferroni correction) were applied. If data did not suffice the assumptions for parametric tests, nonparametric tests (Kruskal-Wallis, followed by Dunn's post hoc pairwise test) were performed. For comparison of two groups, Student's t test (Figure 3D and Figure 3 – figure supplement 1) or Mann-Whitney U test (Figure 7E) were performed.

Bars and error bars represent means and SEM, respectively, in all figures. For all figures, significance corresponds to the following symbols: * $p < 0.05$; ** $p < 0.01$; *** $p < 0.001$; ns: not significant $p>0.05$.

Other information

Funding

Funder	Grant number	Author
JST SPRING	JPMJSP2114	Shun Hiramatsu
JSPS KAKENHI	22H04829	Hiromu Tanimoto
JSPS KAKENHI	20H00519	Hiromu Tanimoto
JSPS KAKENHI	22H05481	Hiromu Tanimoto
JSPS KAKENHI	22KK0106	Hiromu Tanimoto
JSPS KAKENHI	17H01378	Hiromu Tanimoto
JSPS KAKENHI	20H03246	Shu Kondo
JSPS KAKENHI	19KK0383	Nobuhiro Yamagata
JSPS KAKENHI	17H04765	Nobuhiro Yamagata
Takeda Science Foundation		Nobuhiro Yamagata

Author contributions

H.T. and S.H. conceived the project.
H.T. S.H. and N.Y. designed experiments and interpreted results.
S.K. and H.K. designed, generated, and provided transgenic flies.
H.T and C-F. W. supervised experiments.
S.H., K.S. and N.Y. conducted experiments and analyzed data.
H.T., and S.H. drafted the manuscript.
All authors wrote and revised the manuscript.
All authors read and approved the final manuscript.

429 **References**

430 Andretic, R., Kim, Y. C., Jones, F. S., Han, K. A., & Greenspan, R. J. (2008). Drosophila D1
431 dopamine receptor mediates caffeine-induced arousal. *Proceedings of the National*
432 *Academy of Sciences of the United States of America*, *105*(51), 20392–20397.
433 https://doi.org/10.1073/pnas.0806776105

434 Anton, S. E., Kayser, C., Maiellaro, I., Nemec, K., Möller, J., Koschinski, A., Zaccolo, M.,
435 Annibale, P., Falcke, M., Lohse, M. J., & Bock, A. (2022). Receptor-associated independent
436 cAMP nanodomains mediate spatiotemporal specificity of GPCR signaling. *Cell*, *185*(7),
437 1130-1142.e11. https://doi.org/10.1016/j.cell.2022.02.011

438 Aso, Y., Hattori, D., Yu, Y., Johnston, R. M., Iyer, N. A., Ngo, T. T. B., Dionne, H., Abbott, L.
439 F., Axel, R., Tanimoto, H., & Rubin, G. M. (2014). The neuronal architecture of the
440 mushroom body provides a logic for associative learning. *ELife*, *3*, e04577.
441 https://doi.org/10.7554/eLife.04577

442 Aso, Y., Herb, A., Ogueta, M., Siwanowicz, I., Templier, T., Friedrich, A. B., Ito, K., Scholz, H.,
443 & Tanimoto, H. (2012). Three Dopamine pathways induce aversive odor memories with
444 different stability. *PLoS Genetics*, *8*(7). https://doi.org/10.1371/journal.pgen.1002768

445 Aso, Y., Ray, R. P., Long, X., Bushey, D., Cichewicz, K., Ngo, T. T., Sharp, B., Christoforou, C.,
446 Hu, A., Lemire, A. L., Tillberg, P., Hirsh, J., Litwin-Kumar, A., & Rubin, G. M. (2019).
447 Nitric oxide acts as a cotransmitter in a subset of dopaminergic neurons to diversify memory
448 dynamics. *ELife*, *9*, 1–33. https://doi.org/10.7554/eLife.64094

449 Aso, Y., & Rubin, G. M. (2016). Dopaminergic neurons write and update memories with cell-
450 type-specific rules. *ELife*, *5*, 1–15. https://doi.org/10.7554/eLife.16135

451 Aso, Y., Sitaraman, D., Ichinose, T., Kaun, K. R., Vogt, K., Belliart-Guérin, G., Plaçais, P. Y.,
452 Robie, A. A., Yamagata, N., Schnaitmann, C., Rowell, W. J., Johnston, R. M., Ngo, T. T.
453 B., Chen, N., Korff, W., Nitabach, M. N., Heberlein, U., Preat, T., Branson, K. M., … Rubin,
454 G. M. (2014). Mushroom body output neurons encode valence and guide memory-based
455 action selection in Drosophila. *ELife*, *3*(3), e04580. https://doi.org/10.7554/eLife.04580

456 Aso, Y., Siwanowicz, I., Bräcker, L., Ito, K., Kitamoto, T., & Tanimoto, H. (2010). Specific
457 dopaminergic neurons for the formation of labile aversive memory. *Current Biology*, *20*(16),
458 1445–1451. https://doi.org/10.1016/j.cub.2010.06.048

459 Awasaki, T., Lai, S. L., Ito, K., & Lee, T. (2008). Organization and postembryonic development
460 of glial cells in the adult central brain of Drosophila. *Journal of Neuroscience*, *28*(51),
461 13742–13753. https://doi.org/10.1523/JNEUROSCI.4844-08.2008

462 Beaulieu, J. M., & Gainetdinov, R. R. (2011). The physiology, signaling, and pharmacology of

463 dopamine receptors. *Pharmacological Reviews*, *63*(1), 182–217.
464 https://doi.org/10.1124/pr.110.002642
465 Berry, J. A., Phan, A., & Davis, R. L. (2018). Dopamine Neurons Mediate Learning and
466 Forgetting through Bidirectional Modulation of a Memory Trace. *Cell Reports*, *25*(3), 651-
467 662.e5. https://doi.org/10.1016/j.celrep.2018.09.051
468 Bock, A., Annibale, P., Konrad, C., Hannawacker, A., Anton, S. E., Maiellaro, I., Zabel, U.,
469 Sivaramakrishnan, S., Falcke, M., & Lohse, M. J. (2020). Optical Mapping of cAMP
470 Signaling at the Nanometer Scale. *Cell*, *182*(6), 1519-1530.e17.
471 https://doi.org/10.1016/j.cell.2020.07.035
472 Bonanno, S. L., Sanfilippo, P., Eamani, A., Sampson, M. M., Kandagedon, B., Li, K., Burns, G.
473 D., Makar, M. E., Zipursky, S. L., & Krantz, D. E. (2024). Constitutive and conditional
474 epitope-tagging of endogenous G protein coupled receptors in Drosophila . *The Journal of*
475 *Neuroscience*, *44*(33), e2377232024. https://doi.org/10.1523/jneurosci.2377-23.2024
476 Boto, T., Louis, T., Jindachomthong, K., Jalink, K., & Tomchik, S. M. (2014). Dopaminergic
477 modulation of cAMP drives nonlinear plasticity across the Drosophila mushroom body
478 lobes. *Current Biology*, *24*(8), 822–831. https://doi.org/10.1016/j.cub.2014.03.021
479 Boto, T., Stahl, A., Zhang, X., Louis, T., & Tomchik, S. M. (2019). Independent Contributions of
480 Discrete Dopaminergic Circuits to Cellular Plasticity, Memory Strength, and Valence in
481 Drosophila. *Cell Reports*, *27*(7), 2014-2021.e2.
482 https://doi.org/10.1016/j.celrep.2019.04.069
483 Burke, C. J., Huetteroth, W., Owald, D., Perisse, E., Krashes, M. J., Das, G., Gohl, D., Silies, M.,
484 Certel, S., & Waddell, S. (2012). Layered reward signalling through octopamine and
485 dopamine in Drosophila. *Nature*, *492*(7429), 433–437. https://doi.org/10.1038/nature11614
486 Claridge-Chang, A., Roorda, R. D., Vrontou, E., Sjulson, L., Li, H., Hirsh, J., & Miesenböck, G.
487 (2009). Writing Memories with Light-Addressable Reinforcement Circuitry. *Cell*, *139*(2),
488 405–415. https://doi.org/10.1016/j.cell.2009.08.034
489 Cohn, R., Morantte, I., & Ruta, V. (2015). Coordinated and Compartmentalized Neuromodulation
490 Shapes Sensory Processing in Drosophila. *Cell*, *163*(7), 1742–1755.
491 https://doi.org/10.1016/j.cell.2015.11.019
492 Croset, V., Treiber, C. D., & Waddell, S. (2018). Cellular diversity in the Drosophila midbrain
493 revealed by single-cell transcriptomics. *ELife*, *7*, 1–31. https://doi.org/10.7554/eLife.34550
494 Davie, K., Janssens, J., Koldere, D., De Waegeneer, M., Pech, U., Kreft, Ł., Aibar, S., Makhzami,
495 S., Christiaens, V., Bravo González-Blas, C., Poovathingal, S., Hulselmans, G., Spanier, K.
496 I., Moerman, T., Vanspauwen, B., Geurs, S., Voet, T., Lammertyn, J., Thienpont, B., …

Aerts, S. (2018). A Single-Cell Transcriptome Atlas of the Aging Drosophila Brain. *Cell*, *174*(4), 982-998.e20. https://doi.org/10.1016/j.cell.2018.05.057

Deng, B., Li, Q., Liu, X., Cao, Y., Li, B., Qian, Y., Xu, R., Mao, R., Zhou, E., Zhang, W., Huang, J., & Rao, Y. (2019). Chemoconnectomics: Mapping Chemical Transmission in Drosophila. *Neuron*, *101*(5), 876-893.e4. https://doi.org/10.1016/j.neuron.2019.01.045

Dorkenwald, S., Matsliah, A., Sterling, A. R., Schlegel, P., Yu, S.-C., McKellar, C. E., Lin, A., Costa, M., Eichler, K., Yin, Y., Silversmith, W., Schneider-Mizell, C., Jordan, C. S., Brittain, D., Halageri, A., Kuehner, K., Ogedengbe, O., Morey, R., Gager, J., … FlyWire Consortium. (2024). Neuronal wiring diagram of an adult brain. *Nature*, *634*. https://doi.org/10.1101/2023.06.27.546656

Dumartin, B., Caillé, I., Gonon, F., & Bloch, B. (1998). Internalization of D1 dopamine receptor in striatal neurons in vivo as evidence of activation by dopamine agonists. *Journal of Neuroscience*, *18*(5), 1650–1661. https://doi.org/10.1523/jneurosci.18-05-01650.1998

Ehmann, N., Owald, D., & Kittel, R. J. (2018). Drosophila active zones: From molecules to behaviour. *Neuroscience Research*, *127*, 14–24. https://doi.org/10.1016/j.neures.2017.11.015

Felsenberg, J., Jacob, P. F., Walker, T., Barnstedt, O., Edmondson-Stait, A. J., Pleijzier, M. W., Otto, N., Schlegel, P., Sharifi, N., Perisse, E., Smith, C. S., Lauritzen, J. S., Costa, M., Jefferis, G. S. X. E., Bock, D. D., & Waddell, S. (2018). Integration of Parallel Opposing Memories Underlies Memory Extinction. *Cell*, *175*(3), 709-722.e15. https://doi.org/10.1016/j.cell.2018.08.021

Fendl, S., Vieira, R. M., & Borst, A. (2020). Conditional protein tagging methods reveal highly specific subcellular distribution of ion channels in motion-sensing neurons. *ELife*, *9*, 1–48. https://doi.org/10.7554/eLife.62953

Ford, C. P. (2014). The role of D2-autoreceptors in regulating dopamine neuron activity and transmission. *Neuroscience*, *282*, 13–22. https://doi.org/10.1016/j.neuroscience.2014.01.025

Fouquet, W., Owald, D., Wichmann, C., Mertel, S., Depner, H., Dyba, M., Hallermann, S., Kittel, R. J., Eimer, S., & Sigrist, S. J. (2009). Maturation of active zone assembly by Drosophila Bruchpilot. *Journal of Cell Biology*, *186*(1), 129–145. https://doi.org/10.1083/jcb.200812150

Friggi-Grelin, F., Coulom, H., Meller, M., Gomez, D., Hirsh, J., & Birman, S. (2003). Targeted gene expression in Drosophila dopaminergic cells using regulatory sequences from tyrosine hydroxylase. *Journal of Neurobiology*, *54*(4), 618–627. https://doi.org/10.1002/neu.10185

Gao, R., Asano, S. M., Upadhyayula, S., Pisarev, I., Milkie, D. E., Liu, T. L., Singh, V., Graves, A., Huynh, G. H., Zhao, Y., Bogovic, J., Colonell, J., Ott, C. M., Zugates, C., Tappan, S., Rodriguez, A., Mosaliganti, K. R., Sheu, S. H., Pasolli, H. A., … Betzig, E. (2019). Cortical column and whole-brain imaging with molecular contrast and nanoscale resolution. *Science*, *363*(6424). https://doi.org/10.1126/science.aau8302

Gerfen, C. R., & Surmeier, D. J. (2011). Modulation of striatal projection systems by dopamine. *Annual Review of Neuroscience*, *34*, 441–466. https://doi.org/10.1146/annurev-neuro-061010-113641

Han, C., Jan, L. Y., & Jan, Y. N. (2011). Enhancer-driven membrane markers for analysis of nonautonomous mechanisms reveal neuron-glia interactions in Drosophila. *Proceedings of the National Academy of Sciences of the United States of America*, *108*(23), 9673–9678. https://doi.org/10.1073/pnas.1106386108

Han, K. A., Millar, N. S., Grotewiel, M. S., & Davis, R. L. (1996). DAMB, a novel dopamine receptor expressed specifically in Drosophila mushroom bodies. *Neuron*, *16*(6), 1127–1135. https://doi.org/10.1016/S0896-6273(00)80139-7

Handler, A., Graham, T. G. W., Cohn, R., Morantte, I., Siliciano, A. F., Zeng, J., Li, Y., & Ruta, V. (2019). Distinct Dopamine Receptor Pathways Underlie the Temporal Sensitivity of Associative Learning. *Cell*, *178*(1), 60-75.e19. https://doi.org/10.1016/j.cell.2019.05.040

Hanesch, U., Fischbach, K. F., & Heisenberg, M. (1989). Neuronal architecture of the central complex in Drosophila melanogaster. *Cell and Tissue Research*, *257*(2), 343–366. https://doi.org/10.1007/BF00261838

Hearn, M. G., Ren, Y., McBride, E. W., Reveillaud, I., Beinborn, M., & Kopin, A. S. (2002). A Drosophila dopamine 2-like receptor: Molecular characterization and identification of multiple alternatively spliced variants. *Proceedings of the National Academy of Sciences of the United States of America*, *99*(22), 14554–14559. https://doi.org/10.1073/pnas.202498299

Honegger, K. S., Campbell, R. A. A., & Turner, G. C. (2011). Cellular-resolution population imaging reveals robust sparse coding in the drosophila mushroom body. *Journal of Neuroscience*, *31*(33), 11772–11785. https://doi.org/10.1523/JNEUROSCI.1099-11.2011

Huetteroth, W., Perisse, E., Lin, S., Klappenbach, M., Burke, C., & Waddell, S. (2015). Sweet taste and nutrient value subdivide rewarding dopaminergic neurons in drosophila. *Current Biology*, *25*(6), 751–758. https://doi.org/10.1016/j.cub.2015.01.036

Ichinose, T., Kanno, M., Wu, H., Yamagata, N., Sun, H., Abe, A., & Tanimoto, H. (2021). Mushroom body output differentiates memory processes and distinct memory-guided

behaviors. *Current Biology*, *31*(6), 1294-1302.e4. https://doi.org/10.1016/j.cub.2020.12.032

Ichinose, T., & Tanimoto, H. (2016). Dynamics of memory-guided choice behavior in Drosophila. *Proceedings of the Japan Academy Series B: Physical and Biological Sciences*, *92*(8), 346–357. https://doi.org/10.2183/pjab.92.346

Ichinose, T., Tanimoto, H., & Yamagata, N. (2017). Behavioral modulation by spontaneous activity of dopamine neurons. *Frontiers in Systems Neuroscience*, *11*(December), 1–12. https://doi.org/10.3389/fnsys.2017.00088

Jenett, A., Rubin, G. M., Ngo, T. T. B., Shepherd, D., Murphy, C., Dionne, H., Pfeiffer, B. D., Cavallaro, A., Hall, D., Jeter, J., Iyer, N., Fetter, D., Hausenfluck, J. H., Peng, H., Trautman, E. T., Svirskas, R. R., Myers, E. W., Iwinski, Z. R., Aso, Y., … Zugates, C. T. (2012). A GAL4-Driver Line Resource for Drosophila Neurobiology. *Cell Reports*, *2*(4), 991–1001. https://doi.org/10.1016/j.celrep.2012.09.011

Kamiyama, D., Sekine, S., Barsi-Rhyne, B., Hu, J., Chen, B., Gilbert, L. A., Ishikawa, H., Leonetti, M. D., Marshall, W. F., Weissman, J. S., & Huang, B. (2016). Versatile protein tagging in cells with split fluorescent protein. *Nature Communications*, *7*, 1–9. https://doi.org/10.1038/ncomms11046

Kamiyama, R., Banzai, K., Liu, P., Marar, A., Tamura, R., Jiang, F., Fitch, M. A., Xie, J., & Kamiyama, D. (2021). Cell-type-specific, multicolor labeling of endogenous proteins with split fluorescent protein tags in Drosophila. *Proceedings of the National Academy of Sciences of the United States of America*, *118*(23), 1–11. https://doi.org/10.1073/pnas.2024690118

Kanno, M., Hiramatsu, S., Kondo, S., Tanimoto, H., & Ichinose, T. (2021). Voluntary intake of psychoactive substances is regulated by the dopamine receptor Dop1R1 in Drosophila. *Scientific Reports*, *11*(1), 1–10. https://doi.org/10.1038/s41598-021-82813-0

Ke, M. T., Nakai, Y., Fujimoto, S., Takayama, R., Yoshida, S., Kitajima, T. S., Sato, M., & Imai, T. (2016). Super-Resolution Mapping of Neuronal Circuitry With an Index-Optimized Clearing Agent. *Cell Reports*, *14*(11), 2718–2732. https://doi.org/10.1016/j.celrep.2016.02.057

Kim, Y. C., Lee, H. G., & Han, K. A. (2007). D1 dopamine receptor dDA1 is required in the mushroom body neurons for aversive and appetitive learning in Drosophila. *Journal of Neuroscience*, *27*(29), 7640–7647. https://doi.org/10.1523/JNEUROSCI.1167-07.2007

Kittel, R. J., & Heckmann, M. (2016). Synaptic vesicle proteins and active zone plasticity. *Frontiers in Synaptic Neuroscience*, *8*, 1–8. https://doi.org/10.3389/fnsyn.2016.00008

Kohl, J., Ng, J., Cachero, S., Ciabatti, E., Dolan, M.-J., Sutcliffe, B., Tozer, A., Ruehle, S.,

Krueger, D., Frechter, S., Branco, T., Tripodi, M., & Jefferis, G. S. X. E. (2014). Ultrafast tissue staining with chemical tags. *Proceedings of the National Academy of Sciences*, *111*(36), E3805–E3814. https://doi.org/10.1073/pnas.1411087111

Kondo, S., Takahashi, T., Yamagata, N., Imanishi, Y., Katow, H., Hiramatsu, S., Lynn, K., Abe, A., Kumaraswamy, A., & Tanimoto, H. (2020). Neurochemical Organization of the Drosophila Brain Visualized by Endogenously Tagged Neurotransmitter Receptors. *Cell Reports*, *30*(1), 284-297.e5. https://doi.org/10.1016/j.celrep.2019.12.018

Kotowski, S. J., Hopf, F. W., Seif, T., Bonci, A., & von Zastrow, M. (2011). Endocytosis Promotes Rapid Dopaminergic Signaling. *Neuron*, *71*(2), 278–290. https://doi.org/10.1016/j.neuron.2011.05.036

Krashes, M. J., DasGupta, S., Vreede, A., White, B., Armstrong, J. D., & Waddell, S. (2009). A Neural Circuit Mechanism Integrating Motivational State with Memory Expression in Drosophila. *Cell*, *139*(2), 416–427. https://doi.org/10.1016/j.cell.2009.08.035

Kuromi, H., & Kidokoro, Y. (2000). Tetanic stimulation recruits vesicles from reserve pool via a cAMP-mediated process in Drosophila synapses. *Neuron*, *27*(1), 133–143. https://doi.org/10.1016/S0896-6273(00)00015-5

Kuromi, H., & Kidokoro, Y. (2005). Exocytosis and endocytosis of synaptic vesicles and functional roles of vesicle pools: Lessons from the Drosophila neuromuscular junction. *Neuroscientist*, *11*(2), 138–147. https://doi.org/10.1177/1073858404271679

Li, F., Lindsey, J., Marin, E. C., Otto, N., Dreher, M., Dempsey, G., Stark, I., Bates, A. S., Pleijzier, M. W., Schlegel, P., Nern, A., Takemura, S., Eckstein, N., Yang, T., Francis, A., Braun, A., Parekh, R., Costa, M., Scheffer, L., … Rubin, G. M. (2020). The connectome of the adult drosophila mushroom body provides insights into function. *ELife*, *9*, 1–217. https://doi.org/10.7554/eLife.62576

Lin, S., Owald, D., Chandra, V., Talbot, C., Huetteroth, W., & Waddell, S. (2014). Neural correlates of water reward in thirsty Drosophila. *Nature Neuroscience*, *17*(11), 1536–1542. https://doi.org/10.1038/nn.3827

Liu, C., Goel, P., & Kaeser, P. S. (2021). Spatial and temporal scales of dopamine transmission. *Nature Reviews Neuroscience*, *22*(6), 345–358. https://doi.org/10.1038/s41583-021-00455-7

Liu, C., Plaąais, P. Y., Yamagata, N., Pfeiffer, B. D., Aso, Y., Friedrich, A. B., Siwanowicz, I., Rubin, G. M., Preat, T., & Tanimoto, H. (2012). A subset of dopamine neurons signals reward for odour memory in Drosophila. *Nature*, *488*(7412), 512–516. https://doi.org/10.1038/nature11304

Louis, T., Stahl, A., Boto, T., & Tomchik, S. M. (2018). Cyclic AMP-dependent plasticity underlies rapid changes in odor coding associated with reward learning. *Proceedings of the National Academy of Sciences of the United States of America*, *115*(3), E448–E457. https://doi.org/10.1073/pnas.1709037115

Mahr, A., & Aberle, H. (2006). The expression pattern of the Drosophila vesicular glutamate transporter: A marker protein for motoneurons and glutamatergic centers in the brain. *Gene Expression Patterns*, *6*(3), 299–309. https://doi.org/10.1016/j.modgep.2005.07.006

Maiellaro, I., Lohse, M. J., Kittel, R. J., & Calebiro, D. (2016). cAMP Signals in Drosophila Motor Neurons Are Confined to Single Synaptic Boutons. *Cell Reports*, *17*(5), 1238–1246. https://doi.org/10.1016/j.celrep.2016.09.090

Mao, Z., & Davis, R. L. (2009). Eight different types of dopaminergic neurons innervate the Drosophila mushroom body neuropil: Anatomical and physiological heterogeneity. *Frontiers in Neural Circuits*, *3*(JUL), 1–17. https://doi.org/10.3389/neuro.04.005.2009

Mao, Z., Roman, G., Zong, L., & Davis, R. L. (2004). Pharmacogenetic rescue in time and space of the rutabaga memory impairment by using Gene-Switch. *Proceedings of the National Academy of Sciences of the United States of America*, *101*(1), 198–203. https://doi.org/10.1073/pnas.0306128101

Masek, P., Worden, K., Aso, Y., Rubin, G. M., & Keene, A. C. (2015). A dopamine-modulated neural circuit regulating aversive taste memory in drosophila. *Current Biology*, *25*(11), 1535–1541. https://doi.org/10.1016/j.cub.2015.04.027

Miyamoto, T., Slone, J., Song, X., & Amrein, H. (2012). A fructose receptor functions as a nutrient sensor in the drosophila brain. *Cell*, *151*(5), 1113–1125. https://doi.org/10.1016/j.cell.2012.10.024

Nässel, D. R., & Elekes, K. (1992). Aminergic neurons in the brain of blowflies and Drosophila: dopamine- and tyrosine hydroxylase-immunoreactive neurons and their relationship with putative histaminergic neurons. *Cell & Tissue Research*, *267*(1), 147–167. https://doi.org/10.1007/BF00318701

Noyes, N. C., & Davis, R. L. (2023). Innate and learned odor-guided behaviors utilize distinct molecular signaling pathways in a shared dopaminergic circuit. *Cell Reports*, *42*(2), 112026. https://doi.org/10.1016/j.celrep.2023.112026

Owald, D., Felsenberg, J., Talbot, C. B., Das, G., Perisse, E., Huetteroth, W., & Waddell, S. (2015). Activity of defined mushroom body output neurons underlies learned olfactory behavior in Drosophila. *Neuron*, *86*(2), 417–427. https://doi.org/10.1016/j.neuron.2015.03.025

Pavlowsky, A., Schor, J., Plaçais, P. Y., & Preat, T. (2018). A GABAergic Feedback Shapes Dopaminergic Input on the Drosophila Mushroom Body to Promote Appetitive Long-Term Memory. *Current Biology*, *28*(11), 1783-1793.e4. https://doi.org/10.1016/j.cub.2018.04.040

Perisse, E., Owald, D., Barnstedt, O., Talbot, C. B. B., Huetteroth, W., & Waddell, S. (2016). Aversive Learning and Appetitive Motivation Toggle Feed-Forward Inhibition in the Drosophila Mushroom Body. *Neuron*, *90*(5), 1086–1099. https://doi.org/10.1016/j.neuron.2016.04.034

Perkins, L. A., Holderbaum, L., Tao, R., Hu, Y., Sopko, R., McCall, K., Yang-Zhou, D., Flockhart, I., Binari, R., Shim, H. S., Miller, A., Housden, A., Foos, M., Randkelv, S., Kelley, C., Namgyal, P., Villalta, C., Liu, L. P., Jiang, X., … Perrimon, N. (2015). The transgenic RNAi project at Harvard medical school: Resources and validation. *Genetics*, *201*(3), 843–852. https://doi.org/10.1534/genetics.115.180208

Petruccelli, E., Feyder, M., Ledru, N., Jaques, Y., Anderson, E., & Kaun, K. R. (2018). Alcohol Activates Scabrous-Notch to Influence Associated Memories. *Neuron*, *100*(5), 1209-1223.e4. https://doi.org/10.1016/j.neuron.2018.10.005

Pfeiffer, B. D., Ngo, T. T. B., Hibbard, K. L., Murphy, C., Jenett, A., Truman, J. W., & Rubin, G. M. (2010). Refinement of tools for targeted gene expression in Drosophila. *Genetics*, *186*(2), 735–755. https://doi.org/10.1534/genetics.110.119917

Plaçais, P. Y., & Preat, T. (2013). To favor survival under food shortage, the brain disables costly memory. *Science*, *339*(6118), 440–442. https://doi.org/10.1126/science.1226018

Pribbenow, C., Chen, Y. C., Heim, M. M., Laber, D., Reubold, S., Reynolds, E., Balles, I., Alquicira, T. F. d. V., Grimalt, R. S., Scheunemann, L., Rauch, C., Matkovic, T., Rösner, J., Lichtner, G., Jagannathan, S. R., & Owald, D. (2022). Postsynaptic plasticity of cholinergic synapses underlies the induction and expression of appetitive and familiarity memories in Drosophila. *ELife*, *11*, 1–34. https://doi.org/10.7554/eLife.80445

Renger, J. J., Ueda, A., Atwood, H. L., Govind, C. K., & Wu, C. F. (2000). Role of cAMP cascade in synaptic stability and plasticity: Ultrastructural, and physiological analyses of individual synaptic boutons in Drosophila memory mutants. *Journal of Neuroscience*, *20*(11), 3980–3992. https://doi.org/10.1523/jneurosci.20-11-03980.2000

Rice, M. E., & Cragg, S. J. (2008). Dopamine spillover after quantal release: Rethinking dopamine transmission in the nigrostriatal pathway. *Brain Research Reviews*, *58*(2), 303–313. https://doi.org/10.1016/j.brainresrev.2008.02.004

Riemensperger, T., Völler, T., Stock, P., Buchner, E., & Fiala, A. (2005). Punishment prediction

by dopaminergic neurons in Drosophila. *Current Biology*, *15*(21), 1953–1960. https://doi.org/10.1016/j.cub.2005.09.042

Sachidanandan, D., Aravamudhan, A., Mrestani, A., Nerlich, J., Lamberty, M., Hasenauer, N., Ehmann, N., Pauls, D., Seubert, T., Maiellaro, I., Selcho, M., Heckmann, M., Hallermann, S., & Kittel, R. J. (2023). Rab3 mediates cyclic AMP-dependent presynaptic plasticity and olfactory learning. *BioRxiv*, 1–42.

Saito, M., & Wu, C. F. (1991). Expression of ion channels and mutational effects in giant Drosophila neurons differentiated from cell division-arrested embryonic neuroblasts. *Journal of Neuroscience*, *11*(7), 2135–2150. https://doi.org/10.1523/jneurosci.11-07-02135.1991

Sanfilippo, P., Kim, A. J., Bhukel, A., Yoo, J., Mirshahidi, P. S., Pandey, V., Bevir, H., Yuen, A., Mirshahidi, P. S., Guo, P., Li, H. S., Wohlschlegel, J. A., Aso, Y., & Zipursky, S. L. (2024). Mapping of multiple neurotransmitter receptor subtypes and distinct protein complexes to the connectome. *Neuron*, *112*(6), 942-958.e13. https://doi.org/10.1016/j.neuron.2023.12.014

Schindelin, J., Arganda-Carreras, I., Frise, E., Kaynig, V., Longair, M., Pietzsch, T., Preibisch, S., Rueden, C., Saalfeld, S., Schmid, B., Tinevez, J. Y., White, D. J., Hartenstein, V., Eliceiri, K., Tomancak, P., & Cardona, A. (2012). Fiji: An open-source platform for biological-image analysis. *Nature Methods*, *9*(7), 676–682. https://doi.org/10.1038/nmeth.2019

Schlegel, P., Yin, Y., Bates, A. S., Dorkenwald, S., Eichler, K., Brooks, P., Han, D. S., Gkantia, M., Santos, M., Munnelly, E. J., Badalamente, G., Capdevila, L. S., Sane, V. A., Fragniere, A. M. C., Kiassat, L., Pleijzier, M. W., Stürner, T., Tamimi, I. F. M., Dunne, C. R., … Seung, H. S. (2024). Whole-brain annotation and multi- connectome cell typing of Drosophila. *Nature*, *634*(October). https://doi.org/10.1038/s41586-024-07686-5

Scholz-Kornehl, S., & Schwärzel, M. (2016). Circuit Analysis of a *Drosophila* Dopamine Type 2 Receptor That Supports Anesthesia-Resistant Memory. *The Journal of Neuroscience*, *36*(30), 7936–7945. https://doi.org/10.1523/JNEUROSCI.4475-15.2016

Senapati, B., Tsao, C. H., Juan, Y. A., Chiu, T. H., Wu, C. L., Waddell, S., & Lin, S. (2019). A neural mechanism for deprivation state-specific expression of relevant memories in Drosophila. *Nature Neuroscience*, *22*(12), 2029–2039. https://doi.org/10.1038/s41593-019-0515-z

Shin, M., & Venton, B. J. (2022). Fast-Scan Cyclic Voltammetry (FSCV) Reveals Behaviorally Evoked Dopamine Release by Sugar Feeding in the Adult Drosophila Mushroom Body. *Angewandte Chemie - International Edition*, *61*(44), 1–5.

https://doi.org/10.1002/anie.202207399

Siju, K. P., Štih, V., Aimon, S., Gjorgjieva, J., Portugues, R., & Grunwald Kadow, I. C. (2020). Valence and State-Dependent Population Coding in Dopaminergic Neurons in the Fly Mushroom Body. *Current Biology*, *30*(11), 2104-2115.e4. https://doi.org/10.1016/j.cub.2020.04.037

Srivastava, D. P., Yu, E. J., Kennedy, K., Chatwin, H., Reale, V., Hamon, M., Smith, T., & Evans, P. D. (2005). Rapid, nongenomic responses to ecdysteroids and catecholamines mediated by a novel Drosophila G-protein-coupled receptor. *Journal of Neuroscience*, *25*(26), 6145–6155. https://doi.org/10.1523/JNEUROSCI.1005-05.2005

Stahl, A., Noyes, N. C., Boto, T., Botero, V., Broyles, C. N., Jing, M., Zeng, J., King, L. B., Li, Y., Davis, R. L., & Tomchik, S. M. (2022). Associative learning drives longitudinally graded presynaptic plasticity of neurotransmitter release along axonal compartments. *ELife*, *11*, 1–23. https://doi.org/10.7554/eLife.76712

Sugamori, K. S., Demchyshyn, L. L., McConkey, F., Forte, M. A., & Niznik, H. B. (1995). A primordial dopamine D1-like adenylyl cyclase-linked receptor from Drosophila melanogaster displaying poor affinity for benzazepines. *FEBS Letters*, *362*(2), 131–138. https://doi.org/10.1016/0014-5793(95)00224-W

Takemura, S. ya, Aso, Y., Hige, T., Wong, A., Lu, Z., Xu, C. S., Rivlin, P. K., Hess, H., Zhao, T., Parag, T., Berg, S., Huang, G., Katz, W., Olbris, D. J., Plaza, S., Umayam, L., Aniceto, R., Chang, L. A., Lauchie, S., … Scheffer, L. K. (2017). A connectome of a learning and memory center in the adult Drosophila brain. *ELife*, *6*, 1–43. https://doi.org/10.7554/eLife.26975

Tanaka, N. K., Tanimoto, H., & Ito, K. (2008). Neuronal assemblies of the Drosophila mushroom body. *Journal of Comparative Neurology*, *508*(5), 711–755. https://doi.org/10.1002/cne.21692

Tanenbaum, M. E., Gilbert, L. A., Qi, L. S., Weissman, J. S., & Vale, R. D. (2014). A protein-tagging system for signal amplification in gene expression and fluorescence imaging. *Cell*, *159*(3), 635–646. https://doi.org/10.1016/j.cell.2014.09.039

Tempel, B. L., Bonini, N., Dawson, D. R., & Quinn, W. G. (1983). Reward learning in normal and mutant Drosophila. *Proceedings of the National Academy of Sciences of the United States of America*, *80*(5 I), 1482–1486. https://doi.org/10.1073/pnas.80.5.1482

Tsao, C. H., Chen, C. C., Lin, C. H., Yang, H. Y., & Lin, S. (2018). Drosophila mushroom bodies integrate hunger and satiety signals to control innate food-seeking behavior. *ELife*, *7*, 1–35. https://doi.org/10.7554/eLife.35264

769 Turner, G. C., Bazhenov, M., & Laurent, G. (2008). Olfactory representations by Drosophila
770 mushroom body neurons. *Journal of Neurophysiology*, *99*(2), 734–746.
771 https://doi.org/10.1152/jn.01283.2007
772 Vickrey, T. L., & Venton, B. J. (2011). Drosophila dopamine2-like receptors function as
773 autoreceptors. *ACS Chemical Neuroscience*, *2*(12), 723–729.
774 https://doi.org/10.1021/cn200057k
775 Viswanathan, S., Williams, M. E., Bloss, E. B., Stasevich, T. J., Speer, C. M., Nern, A., Pfeiffer,
776 B. D., Hooks, B. M., Li, W. P., English, B. P., Tian, T., Henry, G. L., Macklin, J. J., Patel,
777 R., Gerfen, C. R., Zhuang, X., Wang, Y., Rubin, G. M., & Looger, L. L. (2015). High-
778 performance probes for light and electron microscopy. *Nature Methods*, *12*(6), 568–576.
779 https://doi.org/10.1038/nmeth.3365
780 Vogt, K., Schnaitmann, C., Dylla, K. V., Knapek, S., Aso, Y., Rubin, G. M., & Tanimoto, H.
781 (2014). Shared mushroom body circuits underlie visual and olfactory memories in
782 Drosophila. *ELife*, *3*, e02395. https://doi.org/10.7554/eLife.02395
783 Wagh, D. A., Rasse, T. M., Asan, E., Hofbauer, A., Schwenkert, I., Dürrbeck, H., Buchner, S.,
784 Dabauvalle, M. C., Schmidt, M., Qin, G., Wichmann, C., Kittel, R., Sigrist, S. J., & Buchner,
785 E. (2006). Bruchpilot, a protein with homology to ELKS/CAST, is required for structural
786 integrity and function of synaptic active zones in Drosophila. *Neuron*, *49*(6), 833–844.
787 https://doi.org/10.1016/j.neuron.2006.02.008
788 Williams, J. L., Shearin, H. K., & Stowers, R. S. (2019). Conditional synaptic vesicle markers for
789 drosophila. *G3: Genes, Genomes, Genetics*, *9*(3), 737–748.
790 https://doi.org/10.1534/g3.118.200975
791 Wu, C. -F, Sakai, K., Saito, M., & Hotta, Y. (1990). Giant Drosophila neurons differentiated from
792 cytokinesis-arrested embryonic neuroblasts. *Journal of Neurobiology*, *21*(3), 499–507.
793 https://doi.org/10.1002/neu.480210310
794 Yamagata, N., Hiroi, M., Kondo, S., Abe, A., & Tanimoto, H. (2016). Suppression of Dopamine
795 Neurons Mediates Reward. *PLoS Biology*, *14*(12), 1–16.
796 https://doi.org/10.1371/journal.pbio.1002586
797 Yamagata, N., Ichinose, T., Aso, Y., Plaçais, P.-Y., Friedrich, A. B., Sima, R. J., Preat, T., Rubin,
798 G. M., & Tanimoto, H. (2015). Distinct dopamine neurons mediate reward signals for short-
799 and long-term memories. *Proceedings of the National Academy of Sciences*, *112*(2), 578–
800 583. https://doi.org/10.1073/pnas.1421930112
801 Yao, W. D., Rusch, J., Poo, M. M., & Wu, C. F. (2000). Spontaneous acetylcholine secretion from
802 developing growth cones of Drosophila central neurons in culture: Effects of cAMP-

pathway mutations. *Journal of Neuroscience*, *20*(7), 2626–2637. https://doi.org/10.1523/jneurosci.20-07-02626.2000

Yao, W. D., & Wu, C. F. (2001). Distinct roles of CaMKII and PKA in regulation of firing patterns and K+ currents in Drosophila neurons. *Journal of Neurophysiology*, *85*(4), 1384–1394. https://doi.org/10.1152/jn.2001.85.4.1384

Zhang, J. Z., Lu, T. W., Stolerman, L. M., Tenner, B., Yang, J. R., Zhang, J. F., Falcke, M., Rangamani, P., Taylor, S. S., Mehta, S., & Zhang, J. (2020). Phase Separation of a PKA Regulatory Subunit Controls cAMP Compartmentation and Oncogenic Signaling. *Cell*, *182*(6), 1531-1544.e15. https://doi.org/10.1016/j.cell.2020.07.043

Zhao, M. L., & Wu, C. F. (1997). Alterations in frequency coding and activity dependence of excitability in cultured neurons of Drosophila memory mutants. *Journal of Neuroscience*, *17*(6), 2187–2199. https://doi.org/10.1523/jneurosci.17-06-02187.1997

Zhou, M., Chen, N., Tian, J., Zeng, J., Zhang, Y., Zhang, X., Guo, J., Sun, J., Li, Y., Guo, A., & Li, Y. (2019). Suppression of GABAergic neurons through D2-like receptor secures efficient conditioning in Drosophila aversive olfactory learning. *Proceedings of the National Academy of Sciences of the United States of America*, *116*(11), 5118–5125. https://doi.org/10.1073/pnas.1812342116

821 **Legends**

822 **Figure 1. Co-expression of *Dop1R1* and *Dop2R* genes in adult *Drosophila* brain.**

823 (A and B) The expression of *Dop1R1-T2A-GAL4* and *Dop2R-T2A-GAL4* visualized by *UAS-*
824 *mCD8::GFP*. Maximum-intensity projections of the whole brain.
825 (C) Schematic of the KCs and the MB-innervating dopamine neurons from the PAM and PPL1
826 clusters.
827 (D-E, G-I) Double labelling of *Dop1R1-T2A-LexA* and *Dop2R-T2A-GAL4* expressions by *lexAop-*
828 *rCD2::GFP* (green) and *UAS-CD4::tdTomato* (red), respectively. Dopamine neurons were
829 immunostained with anti-TH antibody (blue). Single optical sections are shown. Cell bodies of
830 the PAM cluster (D), the PPL1 cluster (E), ring neurons projecting to the ellipsoid body (G and
831 H) and ensheathing glia (I) are shown.
832 (F) Schematic of the regions shown in (G-I).
833 Scale bars, 50 µm (A and B), 5 µm (D, E and I), 20 µm (G and H).

834 **Figure 1 – figure supplement 1. Co-expression of Dop1R1 and Dop2R genes in Kenyon cells.**

835 Double labelling of *Dop1R1-T2A-LexA* and *Dop2R-T2A-GAL4* expressions by *lexAop-*
836 *rCD2::GFP* (green) and *UAS-CD4::tdTomato* (red), respectively. Cell bodies of Kenyon cells are
837 shown. A single optical section is shown.
838 Scale bars, 5 µm.

839 **Figure 2. Cell type-specific visualization of endogenous proteins with GFP_{11} tag.**

840 (A) Principle of cell type specific fluorescent labelling of target proteins by GFP_{11} tag. Seven
841 copies of GFP_{11} are fused to the C-terminal of endogenous receptors. GFP_{1-10} and membrane
842 marker CD4::tdTomato are expressed in the target cells by GAL4/UAS system. In the target cells,
843 reconstitution of GFP occurs on the endogenous proteins tagged with GFP_{11}.
844 (B) As an example, DopEcR::GFP_{11} is visualized in KCs using *MB-Switch*, a ligand-inducible
845 GAL4 driver. To activate Gene-Switch, flies were fed with food containing 200 µM RU486 for
846 12 hours before dissection. A merged image of reconstituted GFP (green) and cellular membrane
847 visualized by CD4::tdTomato (magenta). Maximum intensity projection of the whole left MB.
848 (C) The workflow for visualizing subcellular protein enrichment by localization index (LI). A
849 single sagittal section of the MB calyx and peduncle is shown. The ratio of reconstituted GFP to
850 membrane signal is calculated and normalized by the mean of all voxels to provide LI. In the
851 middle image, LI is color-coded so that red represents local receptor enrichment. In the right
852 image, the intensity of LI color is adjusted based on the membrane signal.

853 **Figure 2 – figure supplement 1. GFP_{11}-tagging on Dop1R1 and Dop2R do not affect aversive**
854 **olfactory memory.**

855 To test the functionality of the knock-in alleles, memory of flies carrying homozygous 7xGFP_{11}-
856 tagged Dop1R1 and Dop2R were compared with those without GFP_{11} tags. To induce
857 reconstitution of GFP in Kenyon cells, GFP_{1-10} was expressed under the control of *MB-Switch*.
858 To activate Gene-Switch, flies were fed with RU486 for 3 days before training.
859 Box plots represent the median as the center line, the upper and lower quartiles as the box
860 boundaries, the minimum and maximum values as the whiskers. Dunn's test was performed (N =
861 9-12). ns: not significant $p>0.05$.

862 **Figure 3. Subcellular localization of Dop1R1 and Dop2R in the Kenyon cells.**

863 Subcellular localization of Dop1R1 and Dop2R in the KCs is visualized by GFP_{11}-tag. *MB-Switch*
864 was used to express GFP_{1-10} and CD4::tdTomato in the KCs. To activate Gene-Switch, flies were
865 fed with food containing 200 μM RU486 for 72 hours before dissection.
866 (A) Schematic showing the projection pattern of a α/β KC.
867 (B) Enrichment of Dop1R1 and Dop2R in the MB lobe. Maximum-intensity projections of the
868 lobe (left) and the calyx (middle) are shown in frontal view. The whole left MB are shown in
869 sagittal view (right). Reconstituted GFP signals for both Dop1R1:: and Dop2R::GFP_{11} distributed
870 throughout the MB lobe and the calyx.
871 (C) Visualization by LI showed more pronounced enrichment of Dop2R than Dop1R1 in the lobe.
872 (D) Mean LI of Dop1R1 and Dop2R in the calyx, the peduncle, the α3 and β2 compartment in the
873 lobe. Student's t test was performed to compare LI of Dop1R1 and Dop2R in each region (N =
874 10). Error bars; SEM. $p > 0.05$, ** $p < 0.01$, *** $p < 0.001$, **** $p < 0.0001$, ns: not significant
875 $p > 0.05$.
876 Scalebars, 20 μm (B and C).

877 **Figure 3 – figure supplement 1. Localization index remains stable across different**
878 **experimental batches.**

879 Two experimental batches showed consistent LI for both *Dop1R1::GFP*$_{11}$ and *Dop2R::GFP*$_{11}$
880 measured in any region in the MB. These two batches were conducted on different days and at
881 different times (Zeitgeber time 5 and 9). The same data set was used in Figure 3D.
882 Student's t test was performed to compare the two batches (N = 5). Bars and error bars represent
883 mean and SEM, respectively. ns: not significant $p > 0.05$.

884 **Figure 4. High-resolution imaging revealed the two opposing dopamine receptors existing**
885 **on the presynaptic and postsynaptic sites of Kenyon cells.**

886 (A) Schematic showing the projection pattern of α/β and γ KCs.
887 (B and C) Airyscan images of Dop1R1::rGFP and Dop2R::rGFP in KCs (green) co-labeled with
888 the AZ stained with anti-Brp (magenta). *MB-Switch* was used with 72 hours of RU486 feeding to
889 express GFP_{1-10} and CD4::tdTomato in the KCs. Brp puncta that overlap with CD4::tdTomato
890 signals (cyan) are identified to be presynaptic sites of in KCs (white arrowheads), and those do
891 not overlap are determined to be presynaptic sites of non-KCs (outlined arrows). The synaptic
892 localization of these receptors is similar in the α 3 (B) and γ5 (C) compartments. In the right
893 panels, white squared regions in the left panels are magnified. Scalebars, 5 μm (left), 1 μm (right).
894 (D) Illustration of localization of Dop1R1 and Dop2R to presynaptic and postsynaptic sites in the
895 axon terminal of KCs.

896 **Figure 5. Presynaptic localization of Dop1R1 and Dop2R in Kenyon cells and giant neurons.**

897 (A) Double labelling of dopamine receptors (green) and the AZ of the KCs (magenta). *MB-Switch*
898 was used with 72 hours of RU486 feeding to express GFP_{1-10} and Brp^{short}::mStraw in the KCs.
899 Single focal slices at the α3 compartment are shown. White squares in the left panels are
900 magnified in the right panels. The Brp puncta in KCs were either abutted by the dopamine receptor
901 signals (white arrowheads) or had barely detectable signals nearby (outlined arrowheads). Scale
902 bars, 5 μm (left), 1 μm (right).
903 (B) Punctate Brp expression in a giant neuron culture differentiated from cytokinesis-arrested
904 neuroblasts of *OK371-GAL4/UAS-mCD8::GFP* embryos. Aggregated Brp condensates

905 (magenta) were observed in the neurite terminals of the cells marked with mCD8::GFP (cyan) in
906 the right panel. Scale bars, 20 μm (left), 10 μm (right).
907 (C) Double labelling of dopamine receptors (green) and the AZs (magenta). *Dop1R1::Venus* or
908 *Dop2R::Venus* was crossed with *Brp::SNAP*. In the left panels, giant neurons extending their
909 neurites from the cell body on the left to the right. In the right panels, white squared regions in
910 the left panels are magnified. Scale bars, 10 μm (left), 2 μm (right).

911 **Figure 5 – figure supplement 1. Presynaptic localization of Dop1R1 and Dop2R in γ Kenyon**
912 **cells.**

913 Double labelling of dopamine receptors (green) and the AZ of the KCs (magenta). As in the α3
914 compartment (Figure 5A), both Dop1R1 and Dop2R were found near the AZ of KCs in the γ5
915 compartment.
916 Scale bars, 5 μm (left), 1 μm (right).

917 **Figure 6. Subcellular localization of Dop1R1 and Dop2R in MBON-γ1pedc>αβ.**

918 (A) The projection pattern of MBON-γ1pedc>αβ from the tracing data in FlyWire (Dorkenwald
919 et al., 2024; Schlegel et al., 2024).
920 (B and C) *R83A12-GAL4* was used to express *UAS-GFP$_{1-10}$* and *UAS-CD4::tdTomato* in the PAM
921 neurons.
922 (B) Reconstituted GFP signals (left) of *Dop1R1::GFP$_{11}$* and *Dop2R::GFP$_{11}$* in MBON-
923 γ1pedc>αβ. Maximum-intensity projections of the left MB lobe. Visualization of LI (right)
924 revealing that both Dop1R1 and Dop2R are enriched in the dendritic projection of MBON-
925 γ1pedc>αβ in the γ1 compartment as well as in the presynaptic boutons.
926 (C) Airyscan images of the presynaptic boutons aroundα3 (left) and dendritic projections in the
927 γ1 compartment (right). White squares in the right panels are magnified in the insertion to show
928 the swelling membrane structures with punctate localization of dopamine receptors.
929 Scale bars, 20 μm (B), 5 μm (C), 1 μm (C, insertion).

930 **Figure 7. Subcellular localization of Dop1R1 and Dop2R in dopamine neurons.**

931 (A) Maximum-intensity projection image showing the distribution of presynaptic sites in the
932 PAM neurons. Left panel: *R58E02-GAL4* was used to express mCD8::GFP (magenta) and
933 nSyb::CLIP (magenta). Right panel: Visualization by LI showing enrichment of nSyb signals in
934 the lobe projection of the PAM neurons.
935 (B) Illustrated projection pattern of the PAM neurons. Red puncta on the dendrites indicate the
936 sparse distribution of presynaptic sites in dendrites.
937 (C-F) Subcellular localization of GFP$_{11}$-tagged Dop1R1 and Dop2R in the PAM neurons.
938 *R58E02-GAL4* (C and F) or *R15A04-GAL4* (D and E) was used to express *UAS-GFP$_{1-10}$* and *UAS-*
939 *CD4::tdTomato* in the PAM neurons.
940 (C) Reconstituted GFP signals of *Dop1R1::GFP$_{11}$* and *Dop2R::GFP$_{11}$* in PAM neurons (left).
941 LI visualization revealed the stronger presynaptic enrichment of Dop2R than that of Dop1R1
942 (right). Maximum-intensity projections of the left hemisphere including the whole MB lobe and
943 dendritic projections of the PAM neurons around the MB.
944 (D and E) LI in PAM-β'1 neuron. (D) The presynaptic terminals of PAM-β'1 neurons are shown
945 (dashed line). (E) Mean LI for Dop1R1 and Dop2R in the β'1 (Mann-Whitney U test, N = 9).
946 Error bars; SEM.
947 (F) A single optical slice of the γ5 compartment in the MB lobe obtained using Airyscan. Merged
948 image of reconstituted GFP (green) and CD4::tdTomato (magenta). Insertions are the magnified

949 images of the presynaptic boutons of PAM-γ5 (white squares).
950 Scale bars, 20 μm (A, C, D and F), 5 μm (F, insertion).

951 **Figure 8. Bidirectional modification of dopamine receptor expression in dopamine neurons.**

952 (A) Schematic illustration of the MB projection of the PAM and PPL1 dopamine neurons.
953 (B) Dop1R and Dop2R in the presynaptic terminals of PAM-γ5 after 48 hours of starvation
954 compared with fed state.
955 (C) Quantification of rGFP signal levels in the presynaptic terminals of PAM-γ5 after 0, 10, 24
956 and 48 hours of starvation (n = 6-13).
957 (D) Reconstituted GFP signals of *Dop1R1::GFP*$_{11}$ and *Dop2R::GFP*$_{11}$ in the PPL1 neurons. In
958 the MB projections of the PPL1 neurons, Dop1R1 was detected in only the α3 compartment.
959 Dop2R was found in all MB projections. Maximum-intensity projections of the MB lobe.
960 (E) Dop1R and Dop2R in the presynaptic terminals of PPL1-α3 after 24 hours of starvation
961 compared with fed state.
962 (F) Quantification of rGFP signal levels in the presynaptic terminals of PPL1-α3 after 0, 10 and
963 24 hours of starvation (n = 7-10).
964 Scale bar, 10 μm (B and E), 20 μm (D).
965 Interaction effects between genotypes and starvation time on protein levels were tested by Two-
966 way ANOVA (C and F). Bars and error bars represent mean and SEM, respectively (C and F). **
967 p< 0.01, *** p< 0.001, ns: not significant p>0.05.

968 **Figure 8 – figure supplement 1. Starvation-dependent change of dopamine receptors in**
969 **PAM and PPL1.**

970 (A and C) Dop1R (A) and Dop2R (C) in the presynaptic terminals of PAM-α1, PAM-β2 and
971 PAM-β'1 after 48 hours of starvation compared with fed state.
972 (B and D) Quantification of dopamine receptor levels in the presynaptic terminals of the PAM
973 neurons after 0 (fed), 10, 24 and 48 hours of starvation (n = 6-13).
974 (E) Dop2R in the presynaptic terminals of PPL1-α'2, PPL1-γ1pedc and PPL1-γ2 and after 24
975 hours of starvation compared with fed state.
976 (F) Quantification of Dop2R levels in the presynaptic terminals of the PPL1 neurons after 0 (fed),
977 10 and 24 hours of starvation (n = 7-10).
978 Scale bar, 10 μm (A, C, E). Bars and error bars represent mean and SEM, respectively (B, D, F).
979 * p< 0.05, ** p< 0.01, *** p< 0.001, ns: not significant p>0.05.

980 **Figure 9. The dual dopaminergic feedback regulating starved-state dependent expression of**
981 **appetitive behavior.**

982 (A) A working model showing the role of the dual dopaminergic feedback regulation. In the
983 starved state, increased Dop1R1 in PAM neurons and increased Dop2R in PPL1 neurons changes
984 the balance between the synaptic outputs from these DANs to favor appetitive behavior.
985 (B) According to the model, loss of Dop2R in PPL1 upregulates output from PPL1 to attenuate
986 appetitive behavior in starved flies.
987 (C) Knockdown of Dop2R in the PPL1 neurons by *MB504B-GAL4* reduced 3-hour appetitive
988 memory performance (t-test with Bonferroni correction, n=14-15). Bars and error bars represent
989 mean and SEM, respectively. * p< 0.05.
990

Figure 1

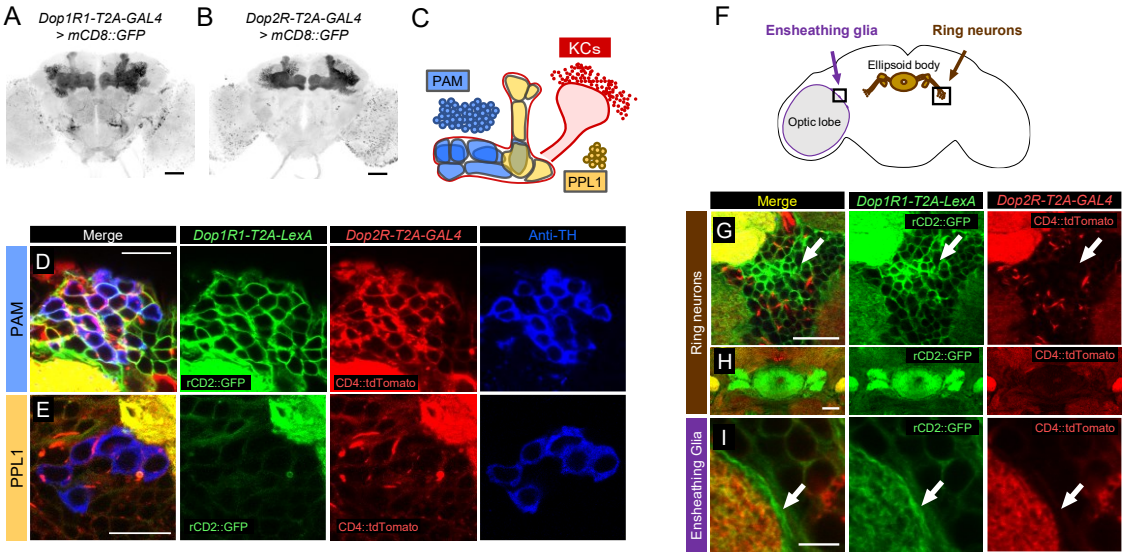

Figure 1 – figure supplement 1

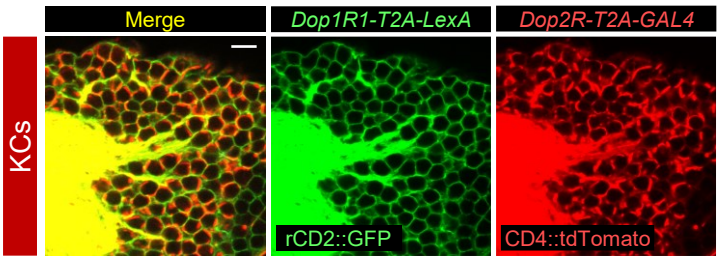

Figure 2

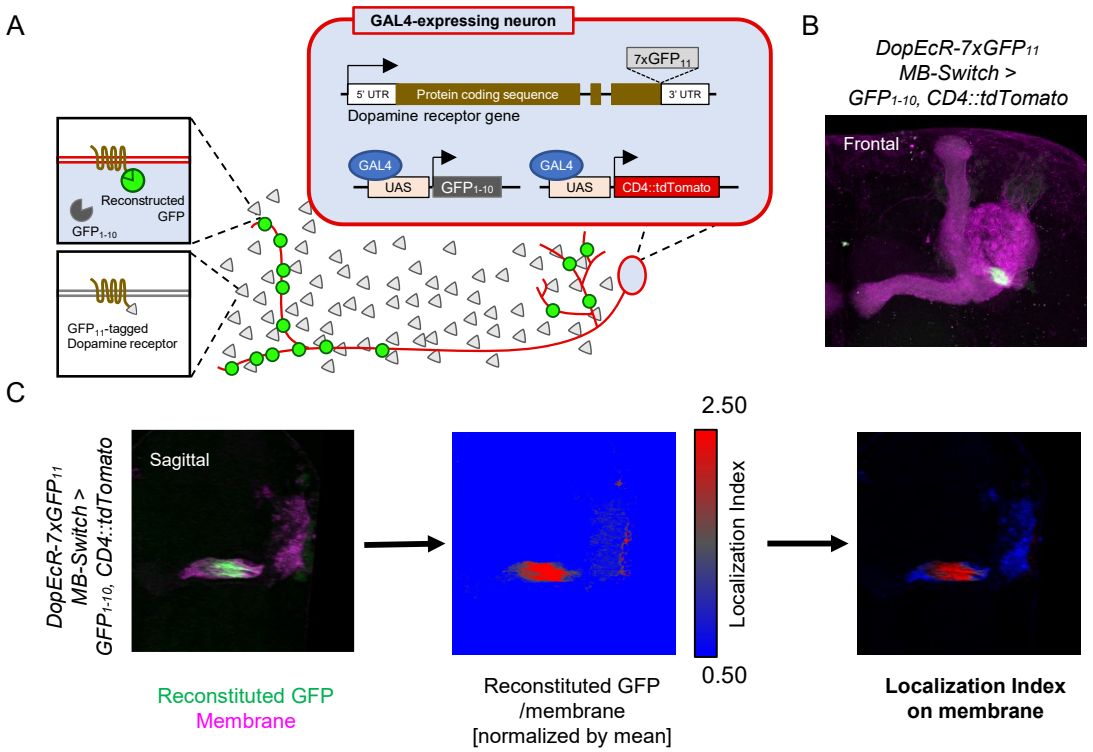

Figure 2 - figure supplement 1

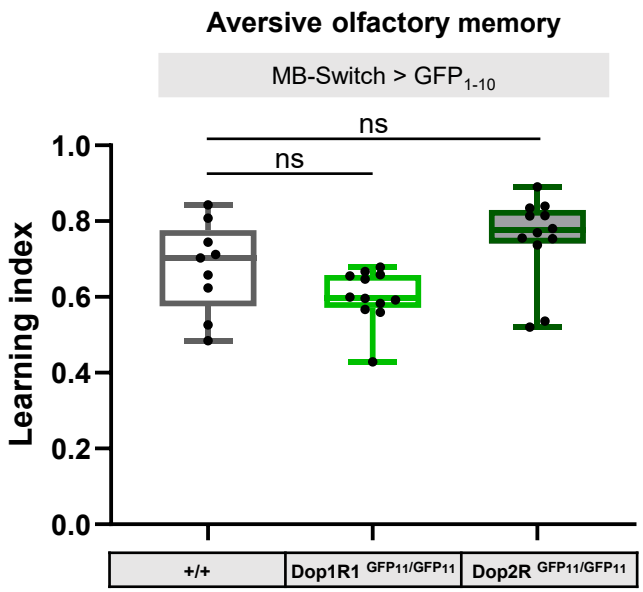

Figure 3

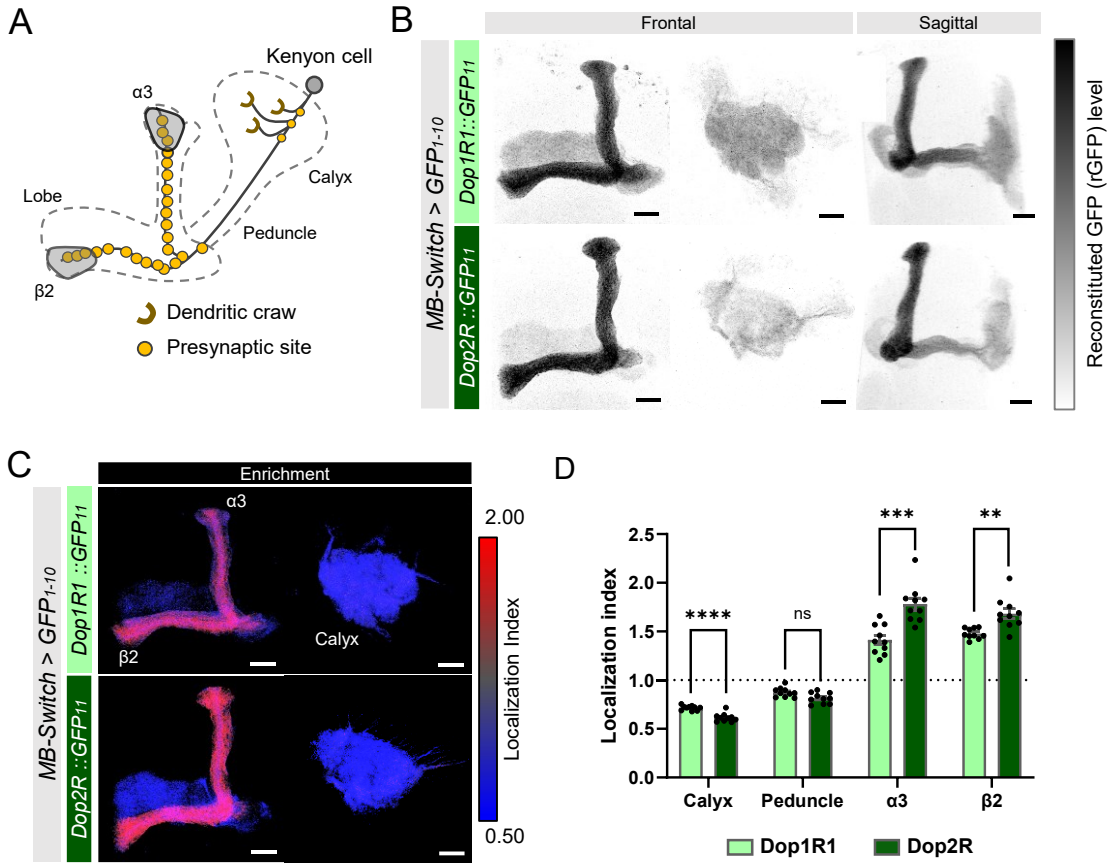

Figure 3 - figure supplement 1

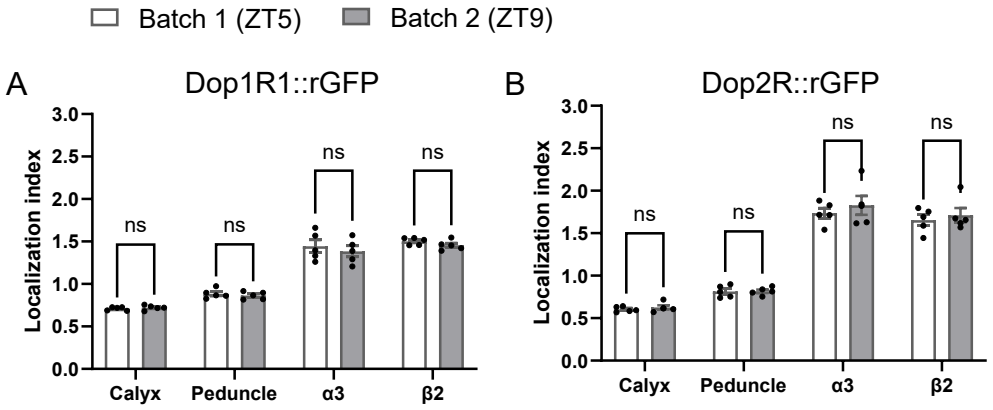

Figure 4

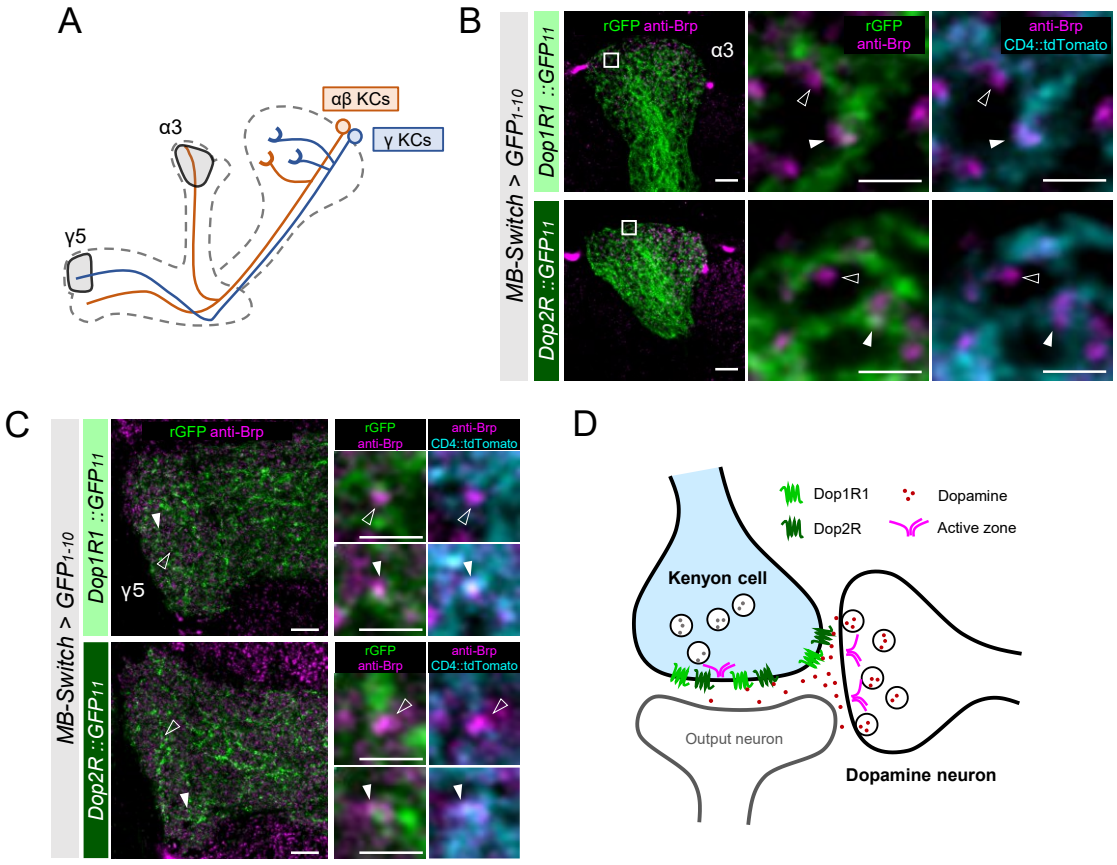
A
αβ KCs
γ KCs
α3
γ5
B
MB-Switch > GFP1-10
Dop1R1 ::GFP11
Dop2R ::GFP11
rGFP anti-Brp
α3
rGFP
anti-Brp
anti-Brp
CD4::tdTomato
C
γ5
D
Dop1R1
Dop2R
Dopamine
Active zone
Kenyon cell
Output neuron
Dopamine neuron

Figure 5

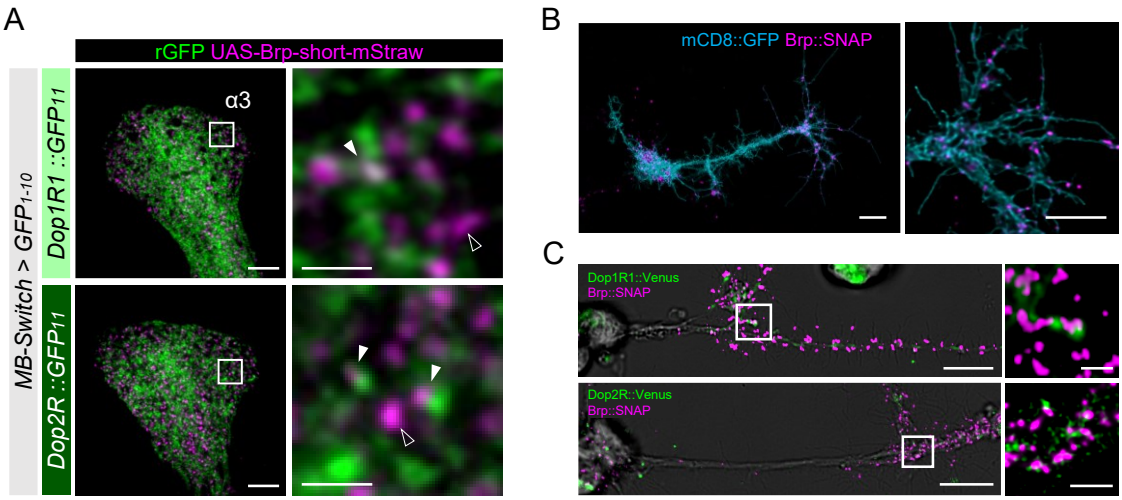

Figure 5 - figure supplement 1

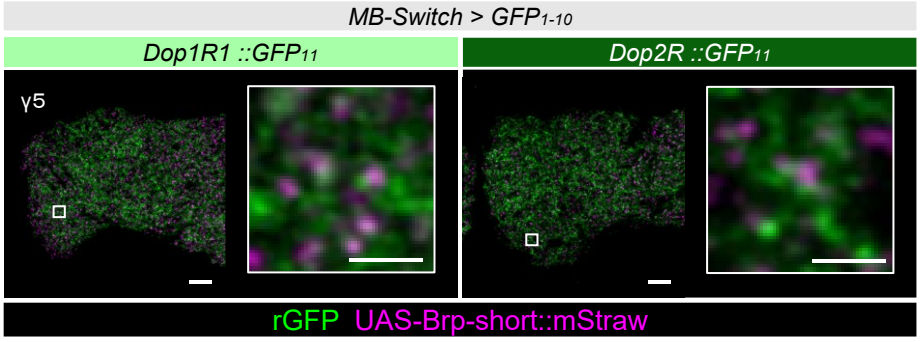

Figure 6

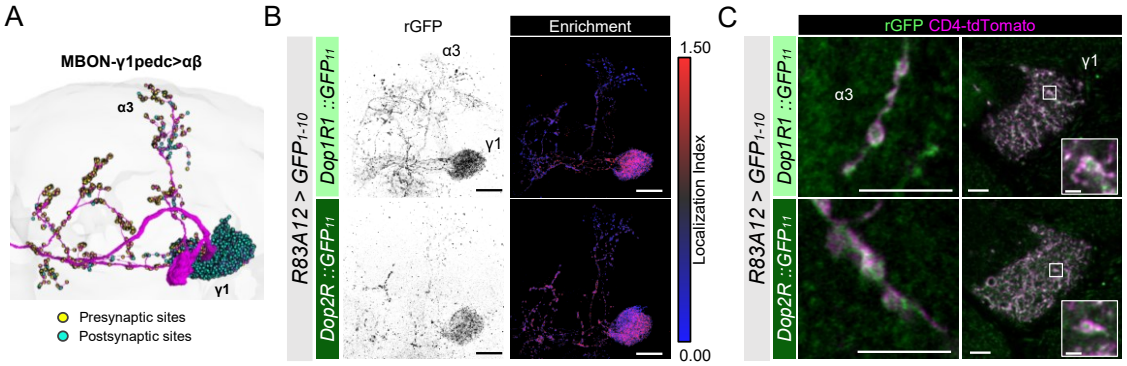
A
MBON-γ1pedc>αβ
α3
γ1
Presynaptic sites
Postsynaptic sites
B
rGFP
Enrichment
R83A12 > GFP1-10
Dop1R1 ::GFP11
Dop2R ::GFP11
α3
γ1
1.50
Localization Index
0.00
C
rGFP CD4-tdTomato
R83A12 > GFP1-10
Dop1R1 ::GFP11
Dop2R ::GFP11
α3
γ1

Figure 7

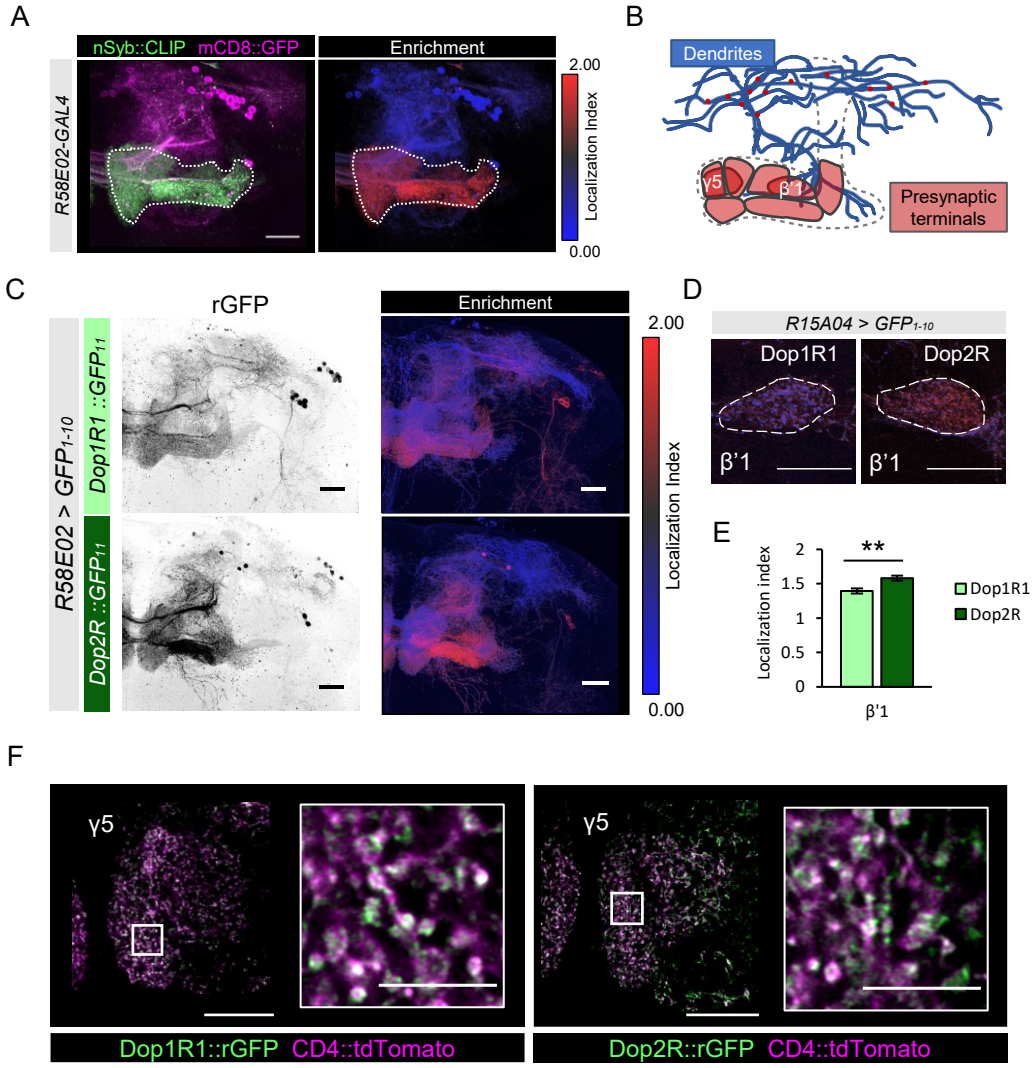
A
nSyb::CLIP mCD8::GFP
Enrichment
R58E02-GAL4
2.00
Localization Index
0.00
B
Dendrites
γ5
β'1
Presynaptic terminals
C
rGFP
Enrichment
R58E02 > GFP1-10
Dop1R1::GFP11
Dop2R::GFP11
2.00
Localization Index
0.00
D
R15A04 > GFP1-10
Dop1R1
Dop2R
β'1
β'1
E
Localization index
2
1.5
1
0.5
0
**
Dop1R1
Dop2R
β'1
F
γ5
γ5
Dop1R1::rGFP CD4::tdTomato
Dop2R::rGFP CD4::tdTomato

Figure 8

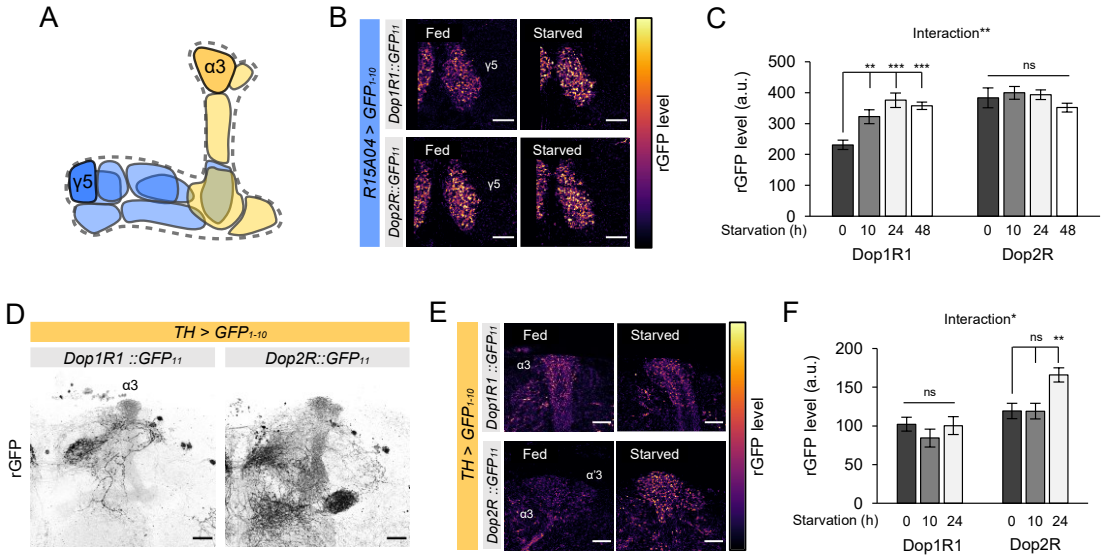
A
α3
γ5
B
R15A04 > GFP1-10
Dop1R1::GFP11
Dop2R::GFP11
Fed
Starved
γ5
rGFP level
C
Interaction**
rGFP level (a.u.)
500
400
300
200
100
0
**
***
***
ns
Starvation (h)
0 10 24 48
0 10 24 48
Dop1R1
Dop2R
D
TH > GFP1-10
Dop1R1 ::GFP11
Dop2R::GFP11
rGFP
α3
E
TH > GFP1-10
Dop1R1 ::GFP11
Dop2R ::GFP11
Fed
Starved
α3
α'3
rGFP level
F
Interaction*
rGFP level (a.u.)
200
150
100
50
0
ns
ns
**
Starvation (h)
0 10 24
0 10 24
Dop1R1
Dop2R

Figure 8 – figure supplement 1

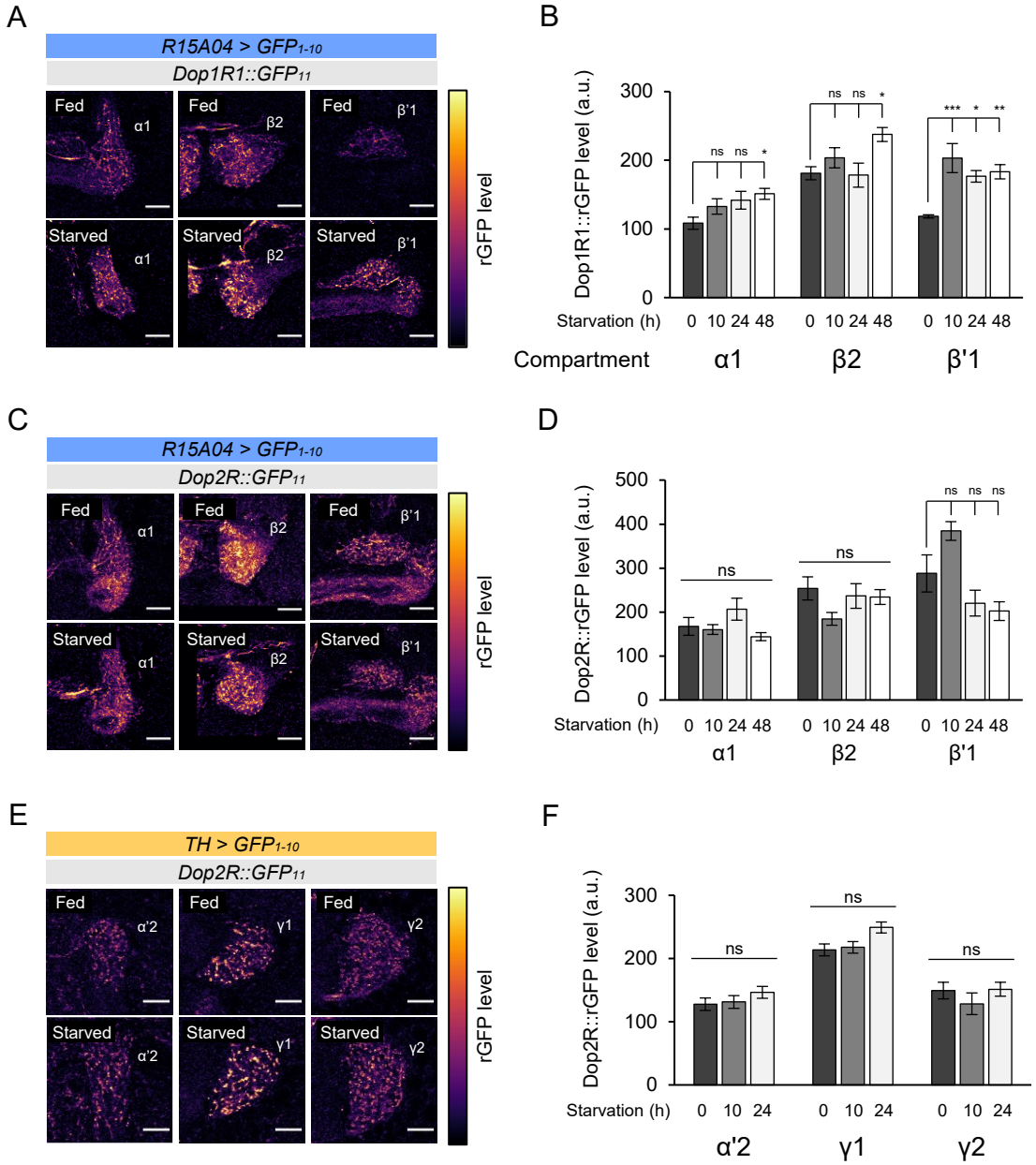

Figure 9

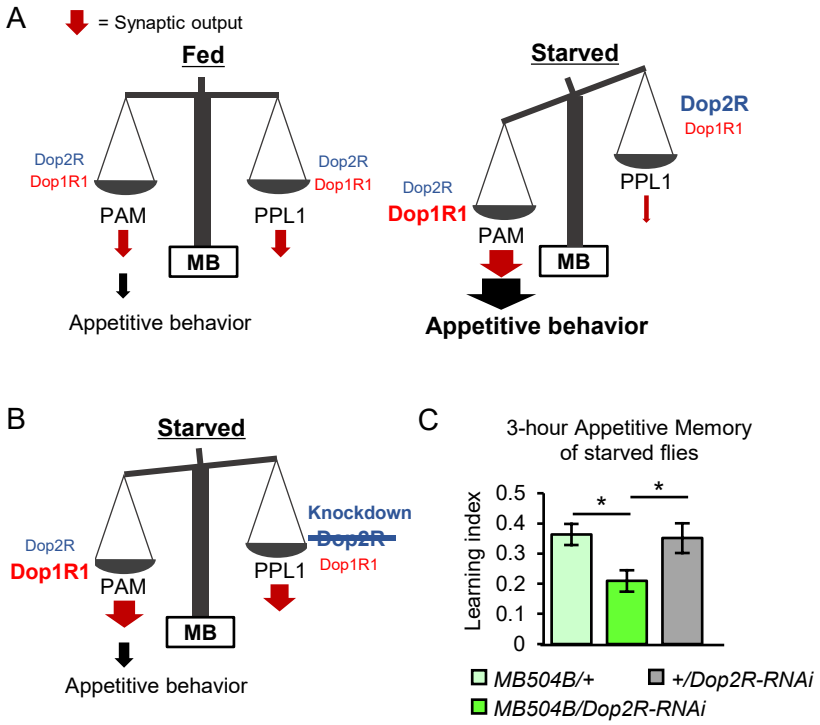
A
= Synaptic output
Fed
Dop2R
Dop1R1
PAM
PPL1
MB
Appetitive behavior
Starved
Dop2R
Dop1R1
PPL1
Dop2R
Dop1R1
PAM
MB
Appetitive behavior
B
Starved
Dop2R
Dop1R1
PAM
PPL1
Knockdown
Dop2R
Dop1R1
MB
Appetitive behavior
C
3-hour Appetitive Memory
of starved flies
Learning index
0.5
0.4
0.3
0.2
0.1
0
*
*
MB504B/+
+/Dop2R-RNAi
MB504B/Dop2R-RNAi